DEGREE PROJECT

Viability of PEEK for high-temperature microvascular composites manufacture

Yago Domínguez Muñoz

Materials Engineering, master's level (120 credits)
2021

Luleå University of Technology
Department of Engineering Sciences and Mathematics

LULEÅ UNIVERSITY OF TECHNOLOGY

ABSTRACT

Microvascular composites are materials with an inner hollow network which allows the circulation of fluids. This functionalizes the composite materials, giving them further applications such as self-healing or active cooling. Some of the already existing microvascular composites are made with fiber reinforced epoxy resin with cavities created by removal of a sacrificial low temperature resistant polymer insert. Current research is focused on the obtention of microvascular composites that can withstand higher service temperatures than epoxy, using polyimide as the high-temperature resin matrix. The aim of this project is to find a suitable sacrificial material that will withstand the higher curing temperatures of the polyimide while allowing its easy removal from the matrix. Three different candidate sacrificial materials were studied for this purpose: PEEK, PPS, and PC.

Preliminary DSC test showed that the melting temperature of the PEEK was close to the range of the chosen resin. PPS melting temperature and PC glass transition temperature were below this range of curing temperatures. TGA test revealed that the degradation suffered by the different materials at the curing temperature of the polyimide was considerably low. A small-scale test mimicking the actual microvascular composite manufacturing conditions was designed to study the actual behavior of the different materials when heated. It was seen that both the PEEK and the PPS could not flow without applying extra pressure for the desired range of temperatures. Furthermore, a scaled model test revealed that there was no visible interaction between the different materials tested and the polyimide resin. The initial study showed that PEEK and PPS are not readily viable to use due to the apparent difficulties to remove them from the composite by just applying heat. PC was also considered not viable for this application since it softened too much a too low temperature.

ACKNOWLEDGEMENTS

I would like to acknowledge all the people who helped me during this project. First, my supervisor, Patrik Fernberg, for his guidance and support during the course of this project. I also wanted to acknowledge Zainab Al-Maqdasi, who helped me with the DSC tests. Tommy Öman, who helped with the TGA tests. Lennar Wallström, who provided me the PPS and PC samples. Lars Frisk, who prepared the glass tubes for my furnace tests. Finally, I would like to thank my family and friends for their unconditional support.

CONTENT

FIGURES & TABLES

Figures

Tables

1. INTRODUCTION

The popularity of composite materials has been increasing due to the numerous advantages that these provide. During the past years, efforts have been made to functionalize these materials. However, the processing of these functional materials often puts the limit on the functionality. The addition of microvascular composites takes inspiration from the biological microvascular systems. In biological systems, such as a tree, these channels are used to circulate a fluid through the organism with different objectives. Imitating this, microvascular channels have been introduced in polymer and composite materials with the goal adding additional functionality to the material.

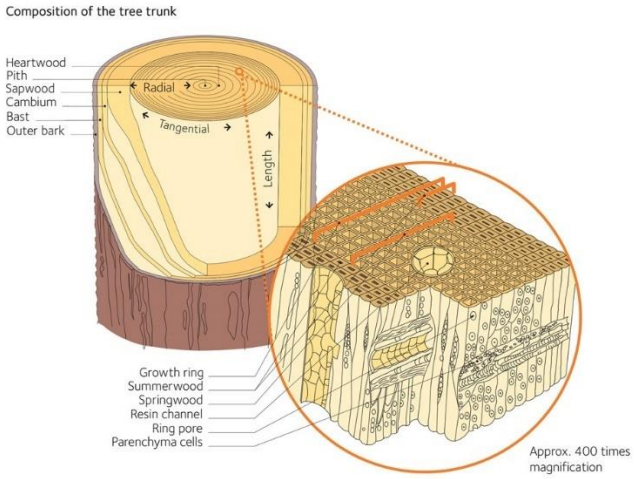

Figure 1. *Tree trunk. Example of a biological microvascular composite. Image from: swedishwood.com*

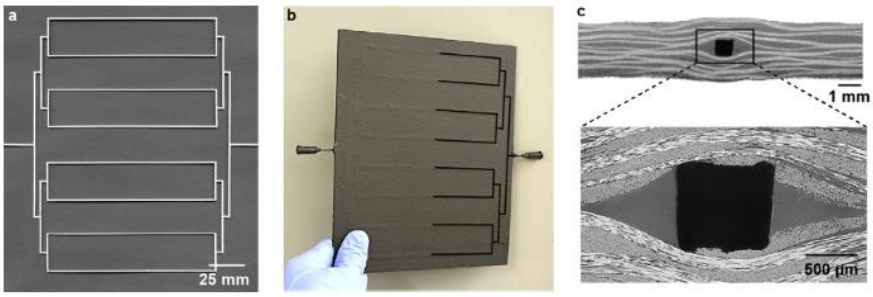

Figure 2. *Carbon fiber/epoxy composite panels with 2D channel networks.*

The idea of this project came out inspired by the work done by S. J. Pety *et al.* [1] consisting on the manufacture of carbon fiber composites with microvascular networks, focused on battery cooling applications. As they say, a big challenge in the increasing industry of the electric vehicle is how to properly package the batteries. The problem of

these batteries is that they require active cooling, to increase the lifetime of the battery and to prevent possible thermal runaway. At the same time, the battery packaging has also to provide structural protection of the battery cell in case of accident. Because of these reasons, there is a need for a system of packaging that can provide both, structural protection, and active cooling, maintaining a light weight.

This is how Pety *et al.* [1] used microvascular carbon fiber composites, achieving simultaneously active cooling and structural protection with a single, lightweight material (Figure 2). This was done using a vaporization of sacrificial components (VaSC) technique to create the composite plate with 2D interconnected and branched microchannel networks inside the material. However, there are different manufacturing techniques previously explored for the creation of microchannels inside a composite material.

2. STATE OF THE ART

2.1 Manufacturing techniques

2.1.1 Non-removable hollow cores

This strategy is one of the simplest that can be found. A group of straight, non-removable hollow tubes made of glass, polymer, or metal is placed between the fiber layers during manufacturing. Once cured, the embedded tubes remain inside the composite, serving as microchannels for different applications. Figure 3 shows schematically the principle of this technique [2].

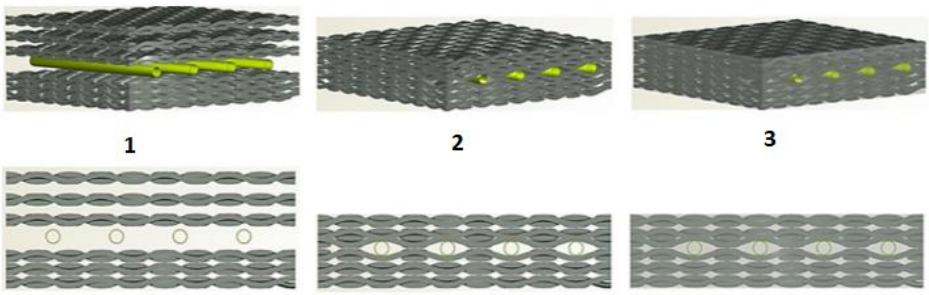

Figure 3. *Schematic diagram for manufacturing techniques based on non-removable hollow cores [2].*

One of the first to attempt to use microchannels was Dry [3][4]. He used hollow glass tubes to make a polymer matrix composite with the ability to self-repair internal microcracks. The samples were subjected to impacts that damaged the epoxy and broke the glass tubes. Then, the content on the tubes leaked, reacting with the damaged area to heal the samples, and restoring lost strength. Other people that work on the same topic were Motuku *et al.* [5]. A new approach was done by Roach [6], who used the microchannels for detecting internal cracks and damages in structures. The microchannels were connected to vacuum and air and linked to different sensors. When damaged, cracks passed through the microchannels, changing the pressure. This change on the pressure was detected by the sensors.

Hollow glass fibers and hollow polymer tubes were also used to crate microchannels, mainly with self-healing applications [2]. Hollow glass tubes, glass fibers and polymer tubes resulted to be a good choice for self-healing applications, but the low thermal conductivity of glass and polymer limited their applications in thermal applications, that is where the metallic tubes were used.

Initially, Motuku *et al.* tried to use copper and aluminum hollow tubes for self-healing applications, but soon marked them as unsuitable [2]. Hemrick *et al.* [7] produced mini-

channels made of aluminum and copper into woven graphite fiber reinforced composites for heat exchange applications. They found that these structures performed well and were appropriate to use in areas where light weight, compact, conformable heat transfer devices were needed. Similar to this, Phillips *et al.* [8] created microvascular channels inserting metallic tubes, but made with stainless steel instead of copper and aluminum.

In general, glass fibers and tubes provided a good control of the shape and size, with a smooth internal surface, which was advantageous for fluid flow. Furthermore, the chemical inertness of the glass allowed the use of different chemicals without interaction with each other. This made the hollow glass tubes and fibers a good candidate for self-healing applications. However, the low thermal conductivity of the glass made the material not suitable for thermal applications. On the other hand, it was the hollow metallic tubes which were not suitable for self-healing applications due their high strength, but were good for heat exchange applications [2].

2.1.2 Removable solid cores

Indistinctly of the material used as a non-removable hollow core, there was always poor resin/channel-surface interface area. This had its contribution in the degradation of the strength of the composites. Thus, some research led to avoid this and start to create microchannels using removable solid preforms. This process is much similar to the one for the non-removable hollow cores. First, the solid preforms are positioned between the fiber layers. After that, the resin infiltration and curing are performed to obtain the composite laminate. Finally, hollow channels are revealed by removing the preforms from the cured laminate [2]. This process is schematically shown in Figure 4.

There are basically two types of solid preforms: polymer fibers and metallic wires. The work of Hamilton *et al.* [9][10] is an example in which this technique was performed, using nylon fibers to create the microchannels inside the composite material. Other example is the work of Wu *et al.* [11], in which trilene monofilament was used to as a removable core. In both cases, the microvascular composites were used for self-healing applications.

On the other hand, Trask and Bond [12] opted for the metallic wires as removable insert. They used an alloy with enough low melting temperature to be removed by heating after curing, but high enough to withstand the curing temperature. Other examples of this manufacturing technique is the work of Norris *et al.* [13][14], who also used a low melting temperature alloy as a removable core.

The system has mainly been used in self-healing applications, as happened with the non-removable cores made of glass or polymer. Despite removable solid cores technique

eliminated the poor channel surface-resin interface area, they created de-shaped channels when soft and low melting temperature solid cores were used [2].

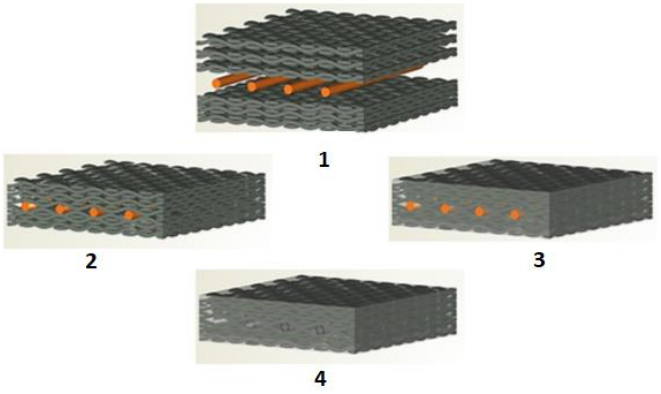

Figure 4. *Schematic illustration for microchannel creation by removable solid cores* [2].

2.1.3 Micromachining/laser processing

Apart from the use of removable and non-removable cores, there are also some studies on the use of micromachining techniques to create microchannels in composite materials. This method had been used previously in metals for cooling applications [2]. One example of the use of micromachining in composite materials is the work of Lima *et al.* [15]. They used a laser to make the microchannels that were used as guidelines for optical fiber. Figure shows the procedure followed in this case. First, a semi-circular channel was laser machined in the two halves of the whole piece. Then, a surface texturing was done for a better bonding between the two parts. Finally, the optical fiber was placed, and the halves were joined.

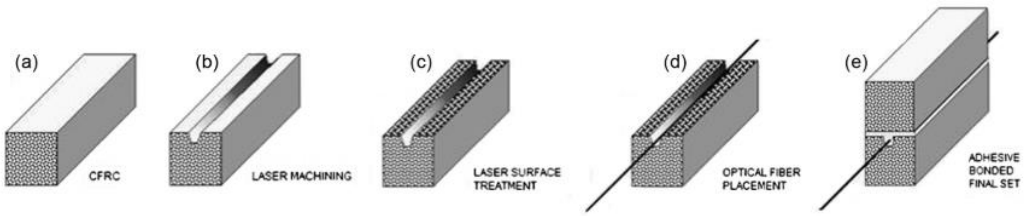

Figure 5. *Schematic of creation microchannels by laser processing (a) composite block, (b) microchannel creation by laser machining, (c) surface texturing by laser, (d) optical fiber placement in the created microchannel and (e) joining of the two half blocks using adhesive [15].*

2.1.4 Direct ink writing

The techniques previously commented only allow the creation straight simple microchannels inside the composite material. Also, these manufacturing techniques were mostly used for self-healing applications, with only a few other applications as self-sensing and thermal applications. To be able to create 2D and 3D patterns with the microchannels networks, direct ink writing was developed [2]. In this process, a fine

nozzle creates 3D patterns by depositing ink while controlled by a computer [16]. Figure shows this process schematically.

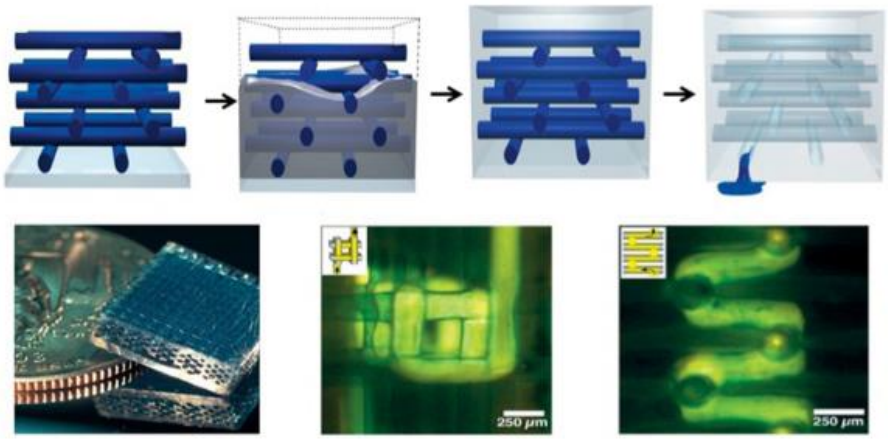

Figure 6. *Schematic representation of direct ink writing*[16].

In their work, Therriault *et al.* [17] were able to create a 3D network using direct ink writing. First, they created the ink network on a cured epoxy substrate. After that, network and substrate were infiltrated with epoxy resin and cured. Once the whole was cured, the ink was removed using heat and vacuum, leaving the hollow 3D network. Other people who used the same manufacturing technique was Toohey *et al.* [18][19]. They created 3D hollow networks that were filled for self-healing applications. There are some other out that also used this technic to produce microvascular composites with self-healing applications. Who used this system for thermal applications was Kozola *et al*. [20]. They found this a good technique to be used for compact and efficient cooling platforms that could be used in different applications.

2.1.5 Electric discharge

Direct ink writing allowed the production of 3D microchannel networks with simple structures, that could be used for self-healing and thermal management applications. Electric discharge technique was developed to produce complex 3D microvascular networks [2]. Electric discharge technique was developed by Huang *et al.* to create branched 3D microchannel networks with a wide range of plastic and composite materials for different applications. This process consists of applying a high electric charge inside a dielectric polymer using electron beam radiation. After that, that energy is discharged in a controlled manner to locally vaporize and fracture the material, leaving the hollow network in a branched arrangement. The diameters obtained with this technique range from 10 µm to 1 mm [21].

The electric discharge was approached in two different ways: grounded contact method and spontaneous discharge method. In the grounded contact approach, after charging the material, the release of energy was made by making contact between the charged material and grounded electrode. In spontaneous discharge method, first a small hole was made on the surface of the substrate. After that, the substrate was charged. Then, the hole was exposed to electron beam to produce internal charge. When the electric discharge reached a critical level, the hole acted as a nucleation site for spontaneous release of energy [21]. Picture show a schematically these two processes and their results.

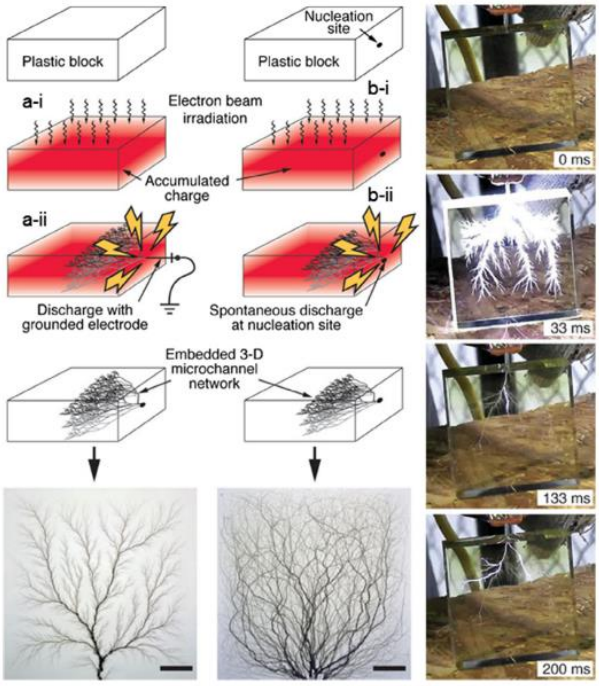

Figure 7. *(a) Schematic of electrostatic discharge phenomena. [21]*

2.1.6 Vaporization of sacrificial components

Although electric discharge technique allows to create complex network structures, these are not well organized. This is solved through the vaporization of sacrificial components. VaSC technique consists in using fiber weave and sacrificial fibers made of polylactic acid (PLA) impregnated with a tin oxalate catalyst (SnOx) [1][22][23]. Usually, the depolymerization temperature of PLA is above 280°C. The addition of the SnOx reduces the depolymerization temperature of the PLA so it can be removed at lower temperatures (around 200°C) and still resist the curing temperature of epoxy. Basically, the VaSC technique is a particular case of removable solid core technique.

The PLA cores are first produced and then placed with the fiber. Then, the resin is infiltrated into the structure. Once the material is cured, the sacrificial PLA is vaporized

at 200°C with the help of vacuum. The PLA is removed from the composite structure, leaving a 3D microchannel network [1][2][22][23]. This technique can be applied in different ways. One way to use this technique is the one performed by Esser-kahn *et al.* [22]. They embedded microchannels in 3D woven composite using VaSC technique for thermal applications, electromagnetic signature, electrical conductivity tuning and chemical reactivity. As show in Figure 8, he PLA fibers used formed part of the weave material prior the resin infiltration. Once the material was fully cured, the PLA was vaporized, and a hollow 3D channel remained inside the composite.

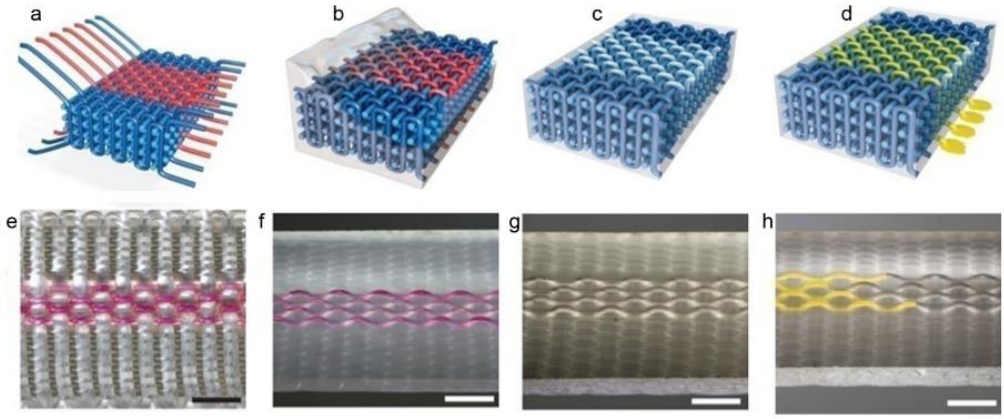

Figure 8. *Schematic diagrams of VaSC [22].*

A different approach to this technique is the one taken by Pety *et al.* in their work [1]. In this case the aim was to obtain a 2D network inside the composite material that allowed the circulation of fluids for cooling applications. To accomplish this, the PLA network needed to be created. First, PLA blended with tin oxalate was pressed into sheets. These sheets were cut with a laser cutter into the 2D network templates. Since the aim of their project was to use the microvascular composite for cooling applications, different network designs were created to find which design had the better efficiency. After that, the composite material was prepared using vacuum-assisted resin transfer molding (VARTM). A total of twelve layers of carbon fiber were stacked in the vacuum bag, with the PLA network template placed between the middle layers of fiber. The layup for the VARTM is schematically shown in FIGURE, from a similar work of Pety [23].

Then, epoxy resin was pulled through the layup. Finally, the resin was cured. Once this process was finished, a plate of a carbon fiber composite containing the PLA template inside was obtained. The plate was cut to the desired size and subject to the VaSC process at 200°C and vacuum. The PLA template was vaporized leaving channel networks that were the inverse replica of the PLA network template. These channels had a cross-section of around 1020 µm x 840 µm, shown in Figure 2.

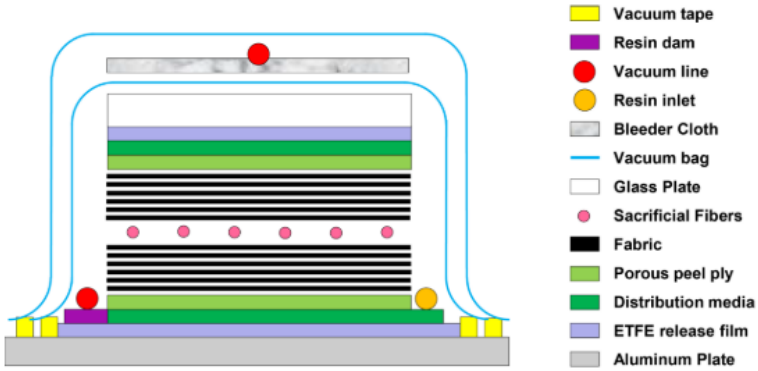

Figure 9. *Double-bag vacuum-assisted resin transfer molding (VARTM) layup for fabricating microvascular composites. Sacrificial fibers are placed between fabric layers and removed/evacuated after cure* [23].

2.2 Sacrificial material

As said before, the idea of this project is to be able to create a microvascular composite material that can withstand higher temperatures than an epoxy resin. In the work previously commented, the material used was an epoxy resin. That epoxy have a maximum glass transition temperature (T_g) of 153°C [24], which would limit its usage in high temperature applications. To be able to achieve a higher service temperature of the microvascular composite, two main materials were considered because of their good thermal properties: polyimide (PI) and polybismaleimide (BMI). The problem emerges when having to decide the material that will be used as the sacrificial material that will be used to have the empty network inside the composite. In the works commented previously, the sacrificial material used was catalyzed PLA.The usage of the PLA is possible in that case because the curing temperature of the epoxy resin is lower than 200°C. To be able to obtain a good microvascularity inside the composite it is necessary that the sacrificial material remains stable during the curing of the material. On the other hand, once the material is fully cured, the sacrificial material must be released from inside the composite with relatively ease.

In this project, the initial main concern when choosing a suitable sacrificial polymer is to find one that can remain stable at the curing temperatures of the chosen matrices. To have an idea of the range of temperatures that the sacrificial polymer would be exposed, the curing temperatures of two different works were used. Table 1 shows the range of curing temperatures used by Fernberg *et al.* [25] in their work about the development of a novel high T_g polyimide-based composite. The polyimide they used is known under the tradename NEXIMID®MHT-R. Two different cycles of curing were performed, but this is not relevant for the moment since the maximum temperature is 370°C in both cycles.

Table 1. *Manufacturing parameters for T650/MHT-R laminates* [25].

	Cycle 1			Cycle 2		
	Time (min)	T (°C)	P (Bar)	Time (min)	T (°C)	P (Bar)
Melt and homogenize inside injection machine	30	240	1	30	240	1
Degass resin using vacuum	10	240	<0.005	10	240	<0.005
Fill mold	~5	290	≤12	~5	320	≤12
Heat mould to cure temperature	30	290–340	12	–	–	–
Isothermal cure	30	340	12	60	320	12
Heat mould to post-cure temperature	30	340–370	12	30	320–370	12
Isothermal post-cure	180	370	12	120	370	12
Cool to de-moulding temperature	720	370–80	1	720	370–80	1

For the bismaleimide, the work of Masari [26] was considered. His work was about the angle change on L-shape carbon fiber reinforced BMI when subjected to different post-curing cycles. The BMI used was named Compimide 50RTM. In this case, the injection of the BMI was done at 110°C so the formulation had a good viscosity that allowed the filling of the mold without starting to polymerize. After the mold was filled, an initial pre-cure step was done at 145°C for 70 min. Finally, the curing of the BMI was done at 180°C for 240 min.

Having said this, the two temperatures that will be considered as maximum curing temperature are 370°C for PI and 180°C for BMI.

2.2.1 Polyaryletherketone

Polyaryletherketones (PAEKs) are a family of semi-crystalline engineering thermoplastics with exceptional thermal stability [27]. Polymers from this family are named referring to the sequence of ether (E) and ketone (K) units in the structure of the molecule. The most common PEAK are the polyaryletheretherketone (PEEK), polyaryletherketone (PEK) and polyaryletherketoneketone (PEKK) [28]. The different combination of ether and ketones has its influence in the chain polarity and rigidity of the molecule. The higher the number of ketone units, higher will be he chain polarity and rigidity. Thus, increasing the ketone to ether (K/E) ratio, thermal properties like T_g will also increase [28][29]. According to this, for the three materials named before, PEKK would be the one with highest T_g and melting temperature (Tm), while PEEK would be the one with the lowest T_g and Tm. However, this can become a problem when melting temperatures become so high that the material becomes difficult to process. Consequently, in some cases, especially for PEKK, the melting point is reduced deliberately without a large effect on the T_g. This is done by introducing non-*para* or non-crystallizable units in the polymer backbone [28].

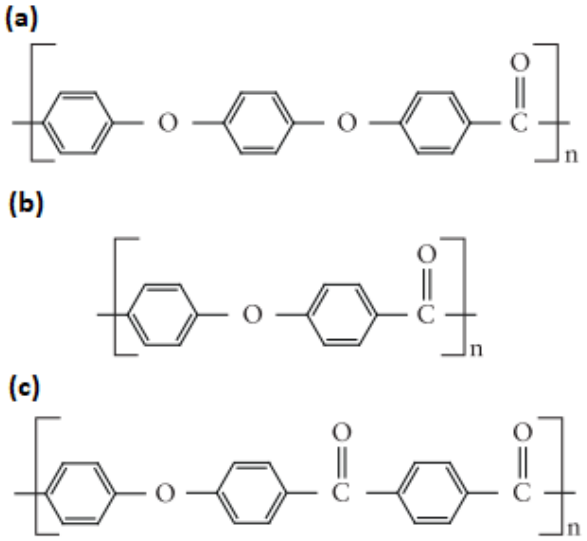

Figure 10. *Repetitive unit of: (a) PEEK, (b) PEK, (c) PEKK* [28].

Because of their thermoplastic nature and their outstanding thermal properties PAEK are considered as a possible polymer to be used for the sacrificial insert for the manufacture of high-temperature microvascular composites. Table 2 shows the different characteristic temperatures of the three different PAEK named before. As can be seen, there are wide ranges of temperatures for either both T_g and T_m because of the multiple commercial formulations that exist. Nevertheless, the melting temperatures are high enough, which means that the material will not degrade while curing the matrix of the composite. At the same time, it would be possible to melt the sacrificial insert made of these materials without damaging the matrix.

2.2.2 Polytetrafluoroethylene (PTFE)

Another high-temperature thermoplastic that has been considered is the polytetrafluoroethylene (PTFE). The PTFE, which molecule is shown in Figure 11, has interesting properties despite its simple molecule. This is attributed to the substitution of the carbon-hydrogen bonds of a linear hydrocarbon chain for carbon-fluorine bonds. These fluorine atoms are what gives the PTFE its incredible properties: is the most chemically resistant organic polymer and is one of the most thermally stable among organic polymers. Its melting point and specific gravity are more than double those of polyethylene (PE), which has the same repetitive unit but with hydrogen instead of fluorine. In this case, PTFE is being considered, along with the PAEK, because of its high melting point [30].

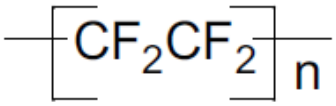

Figure 11. *Repetitive unit of the PTFE* [31].

Table 2 also shows the characteristic temperatures of the PTFE. Once again, the range of melting temperature is high enough to remain stable during the curing of the material and it would be possible to melt the sacrificial insert made of PTFE without damaging the matrix.

Table 2. *Glass transition and melting temperatures for PEEK, PEK and PEKK* [31].

Material	Tg (°C)	Tm (°C)
PEEK	143-158	334-350
PEK	142-154	340-373
PAEK	154-171	304-391
PTFE	117-130	317-345

2.2.3 Polyamide 4, 6 (PA46)

Polyamides (PA) (or nylon) are a family of polymers whose structural units are linked by amide linkage (-NHCO-). These are classified as condensation polymers and the commercially important polyamides are obtained by two basic processes. One is the polycondensation of difunctional monomers using either amido acids or pairs of diamines and carboxylic acids. The other process is the ring-opening polymerization of lactams. Because there are a large variety of polyamides, these have a characteristic nomenclature. Polyamides are commonly identified either as PA X, Y or nylon Z, where X, Y and Z are numbers that signify the number of carbon atoms in the respective structural units. In this case, the polyamide in question is PA46, which means that there are 4 carbon atoms in the diamine backbone unit and 6 carbon atoms in the diacid unit, as shown in Figure.

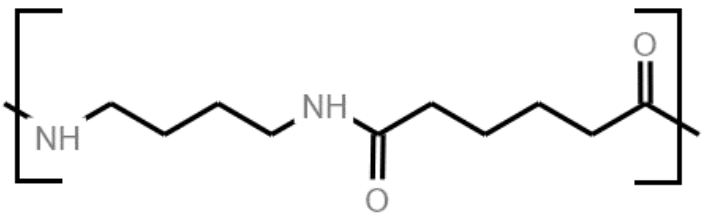

Figure 12. *Repetitive unit of PA46.*

2.2.4 Polyphenylene sulfide (PPS)

Polyphenylene sulfide (PPS) is a semicrystalline polymer with high-temperature resistance. It also has inherent flame resistance and good chemical resistance [32][33]. Even though it is considered a high-temperature polymer, its melting temperature (Table 3) is quite lower compared to the one from PAEKs and PTFE. For this reason, it has been though that this material would be more suitable to use with a BMI matrix composite, which has lower curing temperatures.

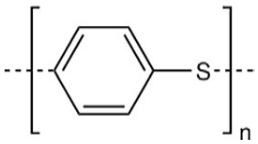

Figure 13. *Repetitive unit of PPS [34].*

2.2.5 Polylactic acid (PLA)

Polylactic acid (PLA) is an aliphatic polyester obtained from lactic acid monomers [35][36]. This polymer is widely for being able to be produced from renewable resources and for being biodegradable. PLA has been previously commented for being the sacrificial material used in some of the mentioned works [1][2][22][23]. In those cases, to be able to remove the PLA from the matrix, it was catalyzed, lowering the decomposition temperature. This allowed extracting the PLA at temperatures at which the matrix would not be damaged.

In this case, because the idea is to work with high temperature resins for the matrix, it would not be necessary to catalyze the PLA. On one hand, the resins can withstand higher temperatures, so it would not suffer damage. On the other hand, because the curing temperatures are higher, the catalyzation of the earlier degradation of the PLA would be an issue. Table shows the glass transition and melting temperatures of the neat PLA.

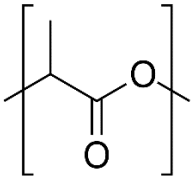

Figure 14. *Repetitive unit of PLA.*

2.2.6 Polycarbonate (PC)

Polycarbonates are a group of polymers with carbonate as linking groups. PCs are classified as aliphatic or aromatic, depending on the accompanying structure of the carbonate group. They are one of the most important engineering plastics. Most of the PC goes to electrical or electronic applications and building industry [37][38]. They have great properties such as optical clarity, great toughness, and high heat capability. PC has a melting temperature (Table 3) high enough to be used as sacrificial material for microvascular composites with BMI matrix.

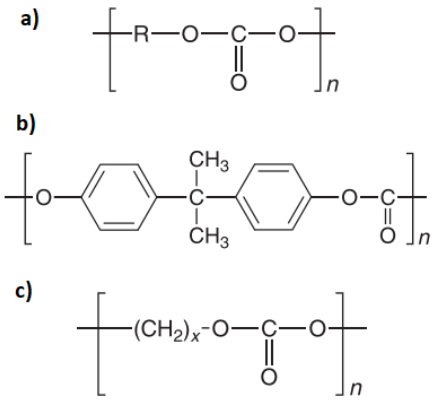

Figure 15. *Repetitive unit of: a) generic PC; b) aromatic PC; c) aliphatic PC* [38].

2.2.7 Polystyrene (PS)

Polystyrene is one of the thermoplastics with highest global demand. It owes its high success to good all-round properties, easy processing and to an environmentally safe production. There are four different varieties of PS: general-purpose PS (GPPS), high impact PS (HIPS), expanded PS (EPS) and syndiotactic PS (sPS) [39]. The one of interest in this case would be the general-purpose PS, since it would be used as sacrificial material and special mechanical properties are not needed.

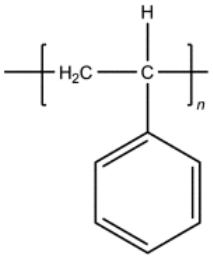

Figure 16. *Repetitive unit of PS [40].*

Table 3. *Glass transition and melting temperatures for sacrificial polymer candidates to be used with BMI resin* [31].

Material	T_g (°C)	T_m (°C)
PA46	43-80	290-295
PPS	74-92	285-295
PLA	55-75	164-178
PC	134-158	255-267
PS	99-108	275

2.3 High temperature resins

2.3.1 Polyimides

Aromatic polyimides can have T_g greater than 316°C. This is the reason why polyimides are of great interest as high temperature resins. The key to achieve this high thermal stability and great high temperature mechanical properties is that the polymer is made with aromatic heterocyclic repeat units, with a minimum aliphatic content, which would contribute to thermal-oxidative instability. Between the different types of aromatic heterocyclic polymers, polyimides have turned to be one of the most successful. The reason behind their good thermal properties is the high aromatic character that can be achieved in polyimides. Also, the inherent rigidity in the repetitive unit contribute in the high Tg which is a key factor for the retention of mechanical properties at high temperature. Two groups of polyimides can be differentiated: condensation polyimides and addition polyimides [41].

2.3.1.1 Condensation polyimides

The process to obtain a polyimide by condensation consists of the reaction of an aromatic dianhydride and an aromatic diamine in a polar solvent such as dimethyl acetamide or N-methyl-2-pyrrolidone (NMP). The problem of this type of synthesis is that the monomeric solution is not suitable for prepregging since the solutions rapidly become too viscous when the range of solids contents in excess reaches 15-20% (the ideal is to have modest viscosities even when the solids contents are in 50-60 wt%).

Thus, in order to be able to obtain a suitable resin for prepregging, the binder solutions need to have the aromatic dianhydride either in tetraacid or diester diacid form, which have open ring structure [41]. The main issue of the condensation polyimides is the evolution of volatile by-products that can lead to porosity inside the material. Examples of commercial condensation polyimides are Skybond®, NR-150 and 3F/36F polyimides.

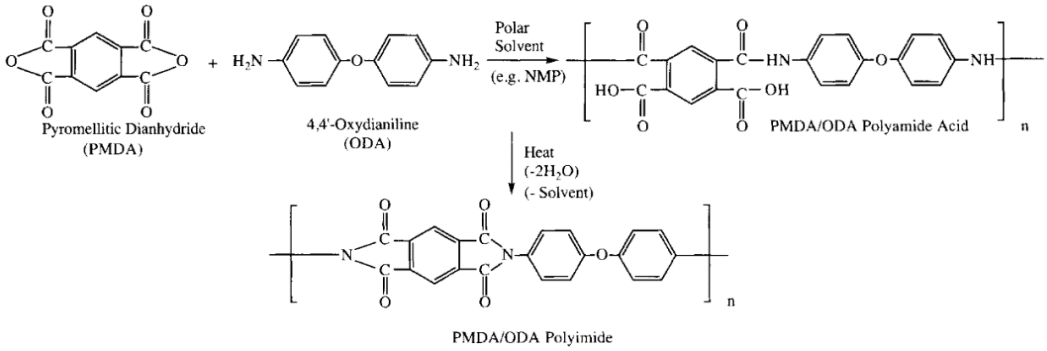

Figure 17. *Typical reaction sequence for a polyimide from a dianhydride and a diamine* [41].

2.3.1.2 Addition polyimides

One important problem in the cure of condensation polyimides is the correct management of the evolution of volatile by-products that lead to porosities inside the material. This issue can be solved using an addition polymerization. This consists in two different steps. Frist, the production *in situ* of an imide oligomer with low enough molecular weight to have a good melt flow that can consolidate when pressure is applied. After that, with further heating, polymerization goes on, obtaining a higher molecular weight polymer without further release of volatile by-products. This is possible to achieve using reactive end groups that can react with each other without releasing volatiles [41].

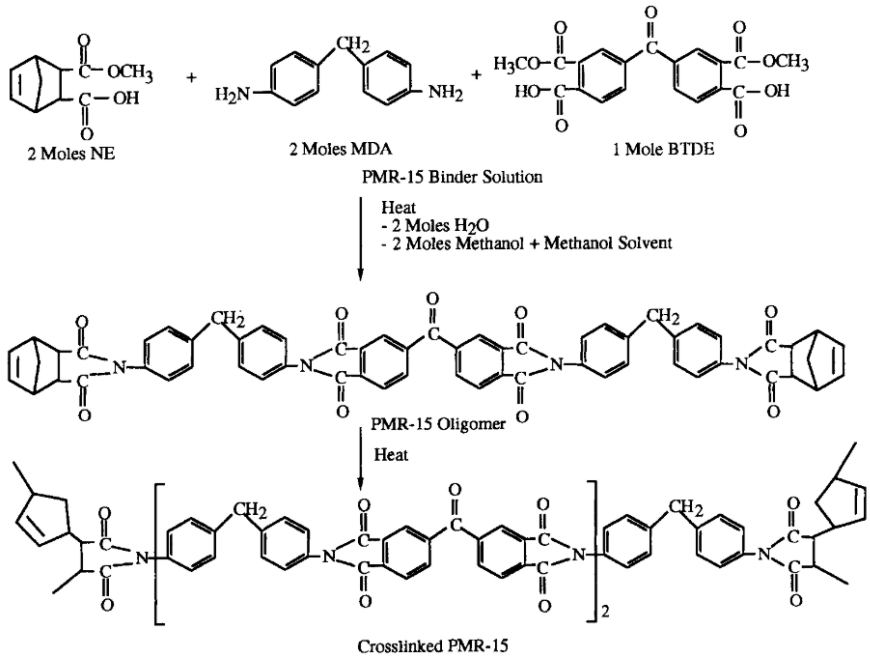

Figure 18. *PMR-15 polymerization chemistry* [41].

However, these improvements have their drawbacks. The toughness of the material can be affected because of the presence of the cross-links. Also, the links produced during the addition polymerizations are generally aliphatic groups, which are susceptible of suffering thermal-oxidative attacks.

Different approaches have been taken with the objective to achieve different trade-offs between processibility and properties. Examples of addition polyimides are PMR-15, PMR-II, V-CAP, CYCAP, AFR700B and TRW-R8XX [41].

2.3.2 Bismaleimides

Bismaleimides (BMI) started to being commercialized during the 1970s as 250-300 °C class resins for circuit board substrates. It was in the early 1980s when it was introduced to the aircraft industry, aiming for higher service temperatures and improved damage tolerance compared to epoxy-based composites. BMI resins have evolved since then, obtaining compression-after-impact rating close to the damage tolerance of thermoplastic resin composites.

The BMI monomers are prepared by reacting aromatic diamines with maleic anhydride in the presence of dehydrating agents. BMI monomers are co-reacted with chain-extending diamines, diallyl bisphenols or dipropenyl phenoxides to develop toughness thanks to the reduced cross link density. This is done because the homopolymers of BMI monomers are too brittle [41].

2.4 Curing

One characteristic that allows the differentiation between different resin systems is the ease to produce a fully cured low void composite having a specified fiber volume. To understand this better, it is interesting to have a look to the Time-Temperature-Transformation (TTT) cure diagrams.

The TTT diagrams provide a framework for understanding the cure process of thermosetting materials. During the curing process, low molecular weight liquid transforms into high molecular weight amorphous solid polymer by chemical reaction. This process is fundamental in the use of thermosets for coatings, adhesives and in composites. As the chemical reaction occurs, the molecular weight and glass transition temperature (T_g) increase. If the reaction is carried out isothermally below the glass transition temperature of fully reacted system ($T_{g\infty}$), the polymer T_g will eventually reach the cure temperature (T_{cure}). For this reason, the curing of the thermoset is done in different steps with increasing temperature. This way it is possible to increase the T_g of the material.

During the isothermal reaction below $T_{g\infty}$, two critical phenomena can occur: gelation and vitrification. The gelation phenomena usually occur fist and is characterized by the formation of material with an infinite molecular weight. Prior to gelation, the system is soluble and fusible. Once the gelation occurs, soluble (sol) and insoluble (gel) materials are both present. As the reaction takes place, the gel fraction (insoluble) increases in expense of the sol (soluble) fraction. As the gelation is reached, the viscosity of the material increases dramatically, and the weight average molecular weight goes to infinity. On the other hand, vitrification is the transformation from liquid or rubbery material to a glassy material. At vitrification, the material solidifies as the chemical reaction extinguishes. Therefore, T_g can equal or exceed T_{cure} [42].

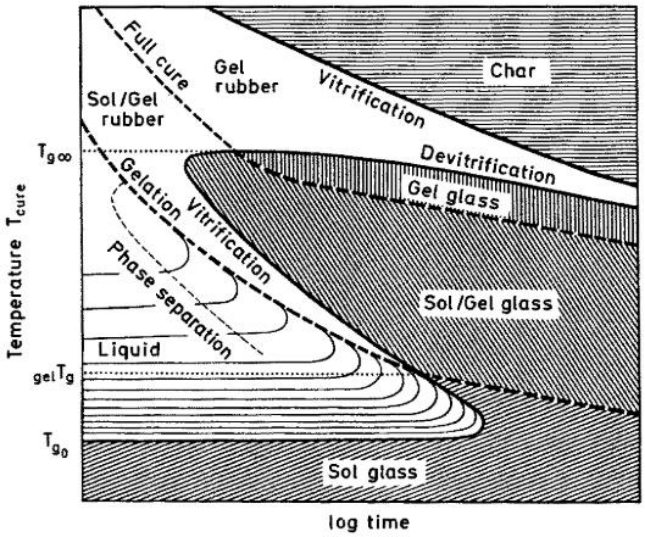

Figure 19. *Schematic time-temperature-transformation (TTT) isothermal cure diagram for a thermosetting system.*

A schematic TTT diagram is shown in Figure 19. It shows different regions found in the thermosetting process. Also, three critical temperatures are shown: Tg_0, $_{gel}T_g$ and $T_{g\infty}$. A "full cure" line can also be seen. This indicates the separation between the sol/gel rubber region and the gel rubber region, and the sol/gel glass region from the gel glass region. It is relevant to note that the temperature vs. time to vitrification has an "S" shape.

Tg_0 is the glass transition temperature of the uncured reactants. At temperatures lower than this one, the system has no reactivity. $_{gel}T_g$, is the temperature at which gelation and vitrification coincide. Between Tg_0 and $_{gel}Tg$, the system will vitrify before gelling. At vitrification below $_{gel}T_g$, the system is of low molecular weight. It will flow with heating and is processable. $T_{g\infty}$ is the maximum glass transition temperature of the system. Between $_{gel}T_g$ and $T_{g\infty}$, the material is initially in the liquid region, is soluble and of low molecular weight. When reacting, the gelation takes place, entering in the sol/gel rubber

region. A miscible binary mixture will form, containing finite molecular weight sol and infinite molecular weight gel. Eventually, T_g will increase until T_{cure}, and vitrification will occur. This decreases considerably the mobility of the molecules, quenching the reaction. When there is not full cure, the vitrified region between ${}_{gel}T_g$ and $T_{g\infty}$ contains both, sol and gel components. The "full cure" line in Figure 19 is the time required for T_g to be equal to $T_{g\infty}$, for any given T_{cure} [42].

In the case at hand, it is important to understand the curing process of the matrix. Since the goal is to obtain a high-temperature microvascular composite, the intention will be to obtain a material with the highest possible T_g. To do so, the material is subjected to curing a post-curing process. It is important to understand these procedures for the material selection. The sacrificial material to be used will be inside the matrix while this one is curing. Thus, that material will also be exposed to the curing temperatures. Depending on the different properties of this material, it is interesting to know the time and temperatures of the curing and post-curing processes. In addition, it is also of interest to know how the time and temperature of these processes can be modified depending on the properties of the sacrificial material, with the minimum change on the final properties of the composite.

2.5 Resin Transfer Molding (RTM)

There are several methods to manufacture composite materials, depending on the type of polymer, the shape of the final piece, size, or type of reinforcement. The following section will focus on RTM since it is a common method according to literature for the preparation of microvascular composite materials [1][23].

The process to produces microvascular composites using RTM consists of the following [43] (This whole process is shown in a simplified way in Figure 4):

- The fiber preform is placed inside the tool. The sacrificial template is place between the two middle layers of fiber. This is schematically shown in Figure 9.
- The mold is heated to the injecting temperature and the resin is pumped into the mold through the preform. The sacrificial material remains on its place, encapsulated in the resin.
- The curing of the material takes place inside the mold.
- Once the resin is cured, it is taken out of the mold and subjected to a post-curing process. Then the sacrificial material is removed from the matrix, leaving the empty channels.

The mold used for the resin transfer molding is usually made of steel or aluminum. However, composite molds can be found for low production batches. The top and bottom halves of the mold need to be stiff enough to resist the pressure of the resin

transfer. In addition, it is necessary to have a resin dispensing equipment for the resin distribution.

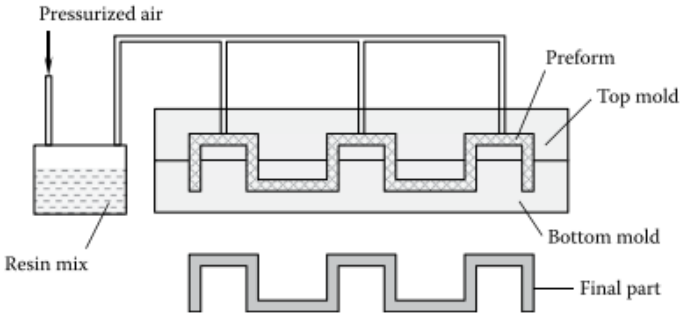

Figure 20. *Schematic representation of the RTM process* [43].

There are several advantages that make RTM such a popular method of composite manufacture. Some of these advantages are [43]:

- Good dimensional tolerances can be achieved, which minimizes the finishing operations.
- Provides good finish in all the sides of the piece.
- Is suitable for making structural parts since the reinforcement can be placed in the mold according to design requirements. Fiber volume fractions up to 65% can be achieved.
- Tooling cost is lower compared to other closed mold processes and is possible to automatize the process.

On the other hand, there are some disadvantages that must be considered:

- The tooling designs is generally complex.
- Might be necessary to run several trials to establish the proper process parameters.

2.6 Differential Scanning Calorimetry

The differential scanning calorimetry (DSC) is a thermal analysis technique that measures the temperatures and heat flows associated with materials as a function of time and temperature. In the microvascular composite manufacture, the sacrificial material remains inside the matrix during the curing process. Also, this sacrificial material is expected to be removed by applying heat. Knowing when the physical

changes associated with the temperature take place is important to know if the material is suitable for the application. With the help of DSC these changes can be studied. If changes like glass transition or melting of the material occur at the range of temperatures of the curing, the loss on the rigidity could cause a change on the sacrificial preform. This could lead to a loss in the control of the microvascular network's shape. For this reason, it is important to know at which temperatures do these changes happen and the impact these have on the material.

2.7 Thermogravimetric Analysis

For the manufacturing of microvascular composites, the sacrificial material needs to be removed after the matrix is cured. This means that the sacrificial material will be inside the matrix while this one is curing. Early degradation of this material while the matrix is curing could cause unwanted defects inside the matrix, such as the apparition of pores due to the liberation of gases, which would suppose a detrimental effect on the properties of the material. An even worse effect caused by an early degradation of the sacrificial material would be the minimization of the material. This would leave empty volumes that would be impregnated by the matrix, losing all the control of the hollow network. TGA test at the curing temperature of the matrix would help to understand how the sacrificial material would behave at the curing temperatures of the matrix. Furthermore, the TGA machine allows the control of the sample environment, which can be helpful to simulate the conditions inside the matrix, where the sacrificial material has no contact with air.

3. EXPERIMENTAL PROCEDURE

3.1 Material

3.1.1 PEEK

PEEK was selected because of its range of melting temperatures and for its good thermal stability.

Specifically, the material used was VICTREX® PEEK 450G, provided by MAPE PLASTICS AB. It was provided as a 28x28x5 mm plate as shown in Figure 21.

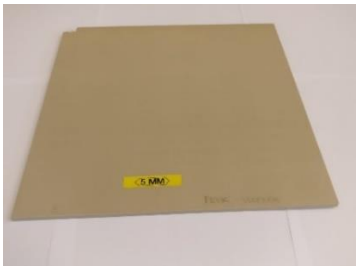

Figure 21. *VICTREX® PEEK 450G plate, size 28x28x5 mm.*

3.1.2 PPS

PPS was the material chosen as a second-tier regarding the thermal properties. PPS has lower thermal stability than PEEK but is still a high-temperature polymer. The PPS used was a RYTON® PPS degree from Phillips Petroleum Company. It was presented as a stick with a size of 270 x 13 x 6 cm, shown in Figure 22.

Figure 22. *RYTON® PPS from Phillips Petroleum Company, size 270x13x6 mm.*

3.1.3 PC

PC was the material chosen with the lowest thermal stability. The PC used was a LEXAN® 9030 by General Electric. It was presented as a sheet with 2 mm thickness, shown in Figure 23.

Figure 23. *LEXAN® 9030 PC sheet with 2 mm thickness. Picture shows a cut taken from the whole sheet.*

3.2 Procedure

The idea was to study the viability of the different candidates as sacrificial materials for high-temperature microvascular composites. During use, the different materials would be exposed to temperature when curing the matrix of the microvascular composite and when removing those materials from the composite. Thus, it was of great interest to observe the behavior of the different materials when heated. To do that, different thermal tests were performed.

3.2.1 Differential Scanning Calorimetry (DSC)

DSC was performed in the METTLER TOLEDO DSC821^{e}. To ease the cutting for the DSC, since the DSC pans are so small, bigger samples were first cut with a DREMEL® 3000. Those bigger samples were later cut with a razor blade into samples small enough to fit in the DSC pans.

For each of the three materials (PEEK, PPS, PC) three different tests were performed with three different heating/cooling rates. Starting at 25°C, the sample was heated up to 400°C. Once this temperature was reached, it was kept at that temperature for 3 min to give time to stabilize and make sure that the 400°C temperature was reached. After these 3 minutes, it was cooled at the same rate down to 25°C. Once again, the sample was kept at that temperature for 3 min. Finally, the second heating was done, once again up to 400°C at the same heating rate. For better visualization, this process is shown in Figure 24. This process was done three times at the heating/cooling rates of 5°C/min, 10°C/min, and 20°C/min, giving the possibility to observe the influence that the heating rate had on the physical changes. All the different tests were done under a nitrogen atmosphere with a pressure of 1 bar and a flow of 80 mL/min.

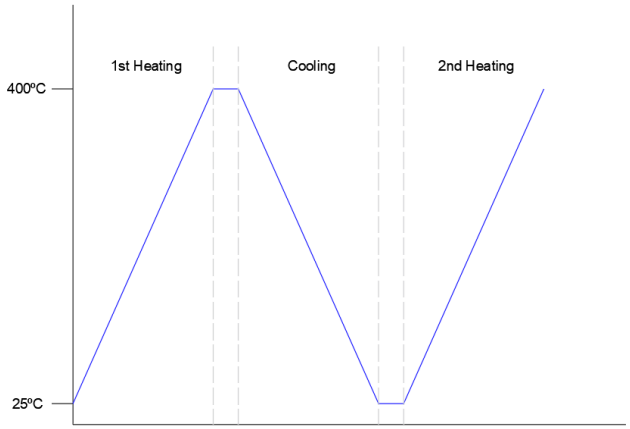

Figure 24. *Method used for the DSC for three different heating/cooling rates. First heating up to 400°C. Keep 400°C for 3 min. Cooling down to 25°C. Keep 25°C for 3 min. Second heating up to 400°C.*

3.2.2 Thermogravimetric Analysis (TGA)

The main idea is to find a suitable material that will be inside the thermosetting matrix while curing. For this reason, it is important to know if the material will degrade at the range of the curing temperatures. An early high degradation would induce the apparition of defects due to the liberation of gases. For this reason, different TGA tests were performed. The thermogravimetric analyzer used was the PerkinElmer® Pyris™ 1 TGA.

These tests consisted of heating a sample from room temperature to 320°C/min, at a heating rate of 20°C/min. After that, the temperature was kept for 1 hour. This process is shown in Figure 25 for better visualization. Wanting to simulate the conditions where the sacrificial material is encapsulated inside the PI matrix, therefore there is no direct contact with air (oxygen), the tests were run in a nitrogen atmosphere. The test was done for each of the candidate materials.

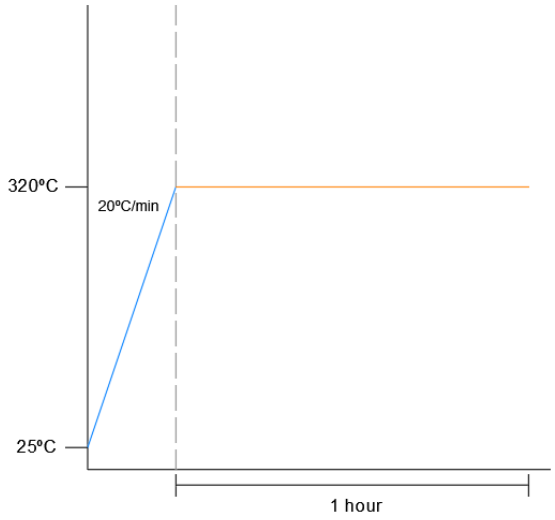

Figure 25. *Method used for the three isothermal TGA tests. First, heating up to the desired temperature (blue). Then, that temperature was kept for 1 h (orange). Both cases in nitrogen atmosphere.*

3.2.3 Small-Scale Tests

Different small-scale model experiments were performed. This was done to investigate if it would be possible to remove the sacrificial material from a small cavity by melting it. The idea was to simulate the conditions at which the sacrificial material would be inside the polyimide matrix. The way of doing this was to introduce the material to be tested inside a longitudinal cavity. After that, the material would be put inside a furnace at a high temperature to see the behavior of the sacrificial material. To simulate the narrow cavity in which the sacrificial material would be, small glass tubes were chosen. Glass was selected as material that could represent the thermally stable polyimide

composite. Also, the tube shape would allow seeing if the materials were able to flow on their own when encapsulated in a constraint space.

A piece of material was cut and put on a watch glass to observe the melting behavior of the material without any constraints (Figure 26A). At the same time, a sample was introduced into one of the previously mentioned glass tubes. These tubes had an internal diameter of 4 mm and were around 10 cm long. The different materials were cut so they could fit inside the tube, as shown in Figure 26B. The furnace used for these tests was the Nabertherm® N 11/HR.

3.2.3.1 PEEK

The samples were put on the furnace. It was heated up to 380°C. Once the furnace reached the desired temperature, it was kept for 90 minutes, and pictures were taken. After that, the furnace was switched off and the material was kept inside for 30 minutes to cool down before removing it from the furnace.

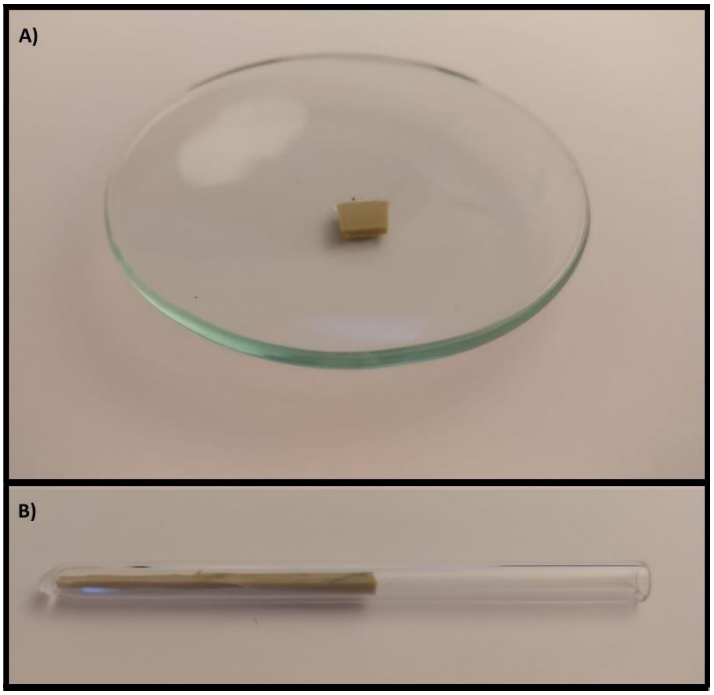

Figure 26.- *Example of the montage for the scale test. A) Piece of material in watch glass to see the melting behavior of the material. B) Piece of material inside the tube. It was cut so it could fit inside the tube.*

The test was repeated a second time with a new sample in a new tube. The previously tested sample in the tube was placed upside down (Figure 27) to see if the material could flow outside the tube by itself.

Figure 27. *Furnace setup of the second test of the PEEK.*

3.2.3.2 PPS and PC

The same procedure was repeated for the PPS and PC with the same initial setup of the tubes. However, since the different materials have different thermal properties, the experimental temperatures were changed depending on the material used. In the case of the PPS, the test temperature was 350°C and in the case of the PC, the experimental temperature was 300°C.

3.2.4 Scale model test

A scale model test was done as a more accurate simulation than the small-scale test. In this case, the objective was to see if there was any interaction between the resin and the sacrificial material. For this purpose, NEXIMID® MHT-R polyimide resin was used. Fragments of the resin were milled into a powder with a porcelain mortar Figure 28. It is important to point out that the resin used was not brand new. The resin used was from non-cured residues from the RTM machine cylinder. This means that the resin used had already been melted before. However, it had not been cured.

The powder was then introduced into three glass tubes with a sample of each of the different tested materials (PEEK, PPS, PC). The glass tubes used were the same size as the ones used for the small-scale test. The powder was placed leaving the sample of the different tested materials in the middle. Enough powder was placed just not to cover the tested samples, as can be seen in Figure 29.

The furnace (Heraeus® D-6450 Hanau) was heated up to 250°C, which was a temperature slightly higher than the melting point of the resin. The objective of this was to melt the resin, being able to encapsulate the different materials inside the resin that would be sued for the matrix. Once the furnace reached the temperature, the samples were placed, and a vacuum was applied. The main reason to use a vacuum was to make sure that any volatile gases released from the resin were removed. After that, the

samples were left inside the furnace for 1 hour. After the samples were removed from the furnace, the process was repeated once more. More powder was introduced in the tubes, and it was put into the furnace once again, at 250°C for 1 hour. In addition, one more PEEK sample was prepared and put into the furnace with the rest of the samples.

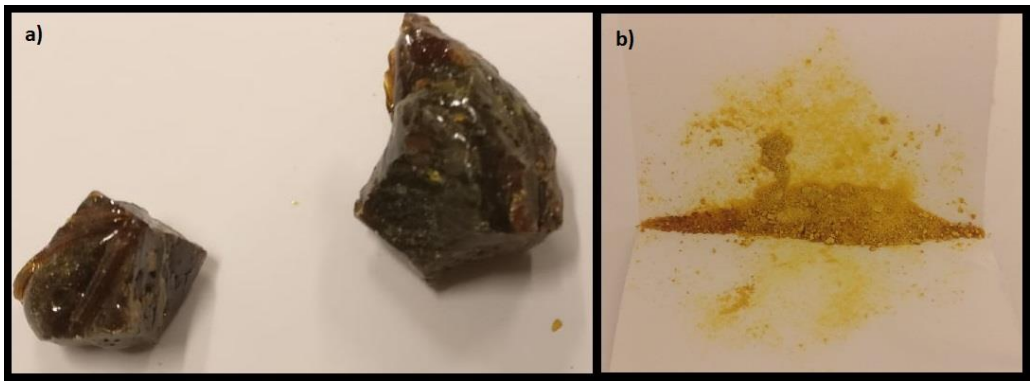

Figure 28.- *NEXIMID® MHT-R resin for the scale model test. a) Resin stones. b) Resin powder after crushing the stones with a porcelain mortar.*

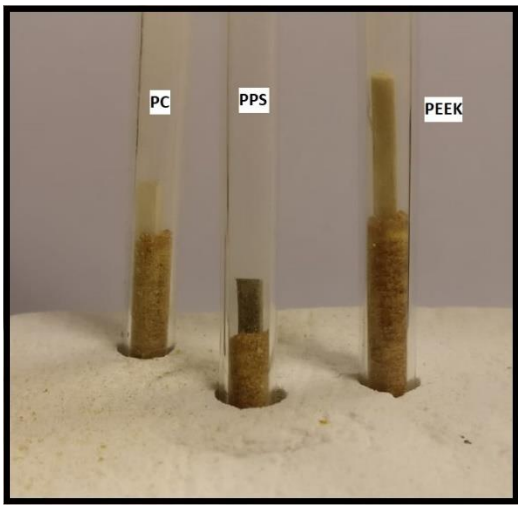

Figure 29. *Samples in the tube filled with powder before the test.*

Once the samples were out of the furnace, the bottom tip of the three initial tubes was cut using the Secoom-10 precision cutting machine and mounted in epoxy resin (EpoFix) to watch in the optical microscope. The extra PEEK sample was placed in the furnace (Nabertherm® N 11/HR) to cure the resin at 340°C for 1 hour. After that, the sample was cut and mounted the same way as the other samples. Finally, the different samples were looked at in the microscope (Zeiss Axioskop) to ensure that there was no interaction between the two materials.

4. REULTS & DISCUSSION

4.1 Differential Scanning Calorimetry

The objective of the DSC test was to locate the glass transition temperature (Tg) and melting temperature (T_m) of the different materials. There was also an interest in the degree of crystallinity. As explained, the tests consisted of first heating, cooling, and second heating. All of these were done at the same heating/cooling rate.

4.1.1 PEEK

Figure 30 shows the DSC result for the PEEK test done with a heating rate of 10°C/min. The scanning results of the three DSC tests for the PEEK, including the tests with heating rates of 5°C/min and 20°C/min, are shown in a bigger scale in the appendix (Figure A1 - Figure A3). The first thing to be observed was the subtlety of the T_g peaks. They were difficult to notice. Is that so that even the program could not properly identify the T_g peak for the second heating at 5°C. On the other hand, the melting peaks, as well as the crystallization peak, were easy to define. In the case of the second heating, the melting onset extended to lower temperatures, making it more difficult to define the baseline for the enthalpy calculation.

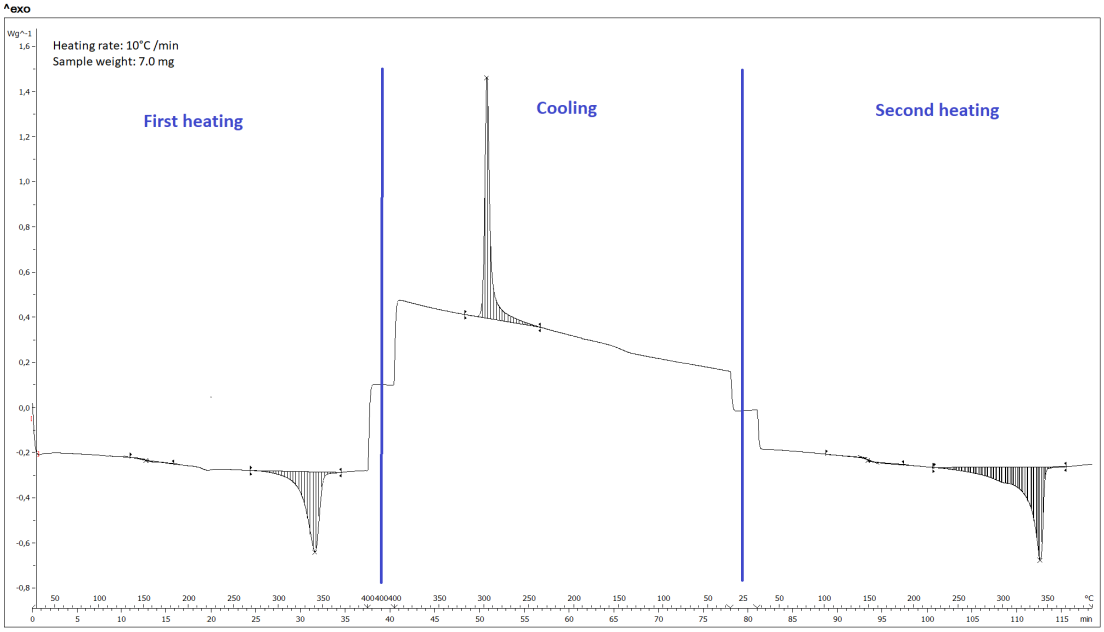

Figure 30. *DSC results for a PEEK sample with a heating/cooling rate of 10°C/min. For better visualization, the same image is shown in Figure A2 in a bigger scale.*

Table 4 shows values of the glass transition temperature, melting temperature, crystallization enthalpy, and degree of crystallinity, extracted from the same tests as the ones shown in Figure A1 - Figure A3. There is a considerable difference in the T_g middle value depending on the heating rate. This happens either for the first or the second heating. When increasing from 5°C/min to 10°C/min, the value of the T_g dropped more than 10°C. With a higher increase in the heating rate, from 10°C/min to 20°C/min, this difference was even more significant, dropping the T_g more than 30°C.

Table 4.- *Glass transition temperature, melting temperature, crystallization enthalpy and degree of crystallinity of the PEEK, extracted from the DSC curves for three different heating rates (Figure A1 -* Figure A3*).*

	Unit	5°C/min	10°C/min	20°C/min
T_g [1st heating]	°C	167.2	154.9	123.3
T_m (peak) [1st heating]	°C	341.2	340.9	342.6
Crystallization enthalpy	J/g	- 41.6	- 40.1	- 31.9
Degree of crystallinity	%	32.0	30.8	24.5
T_g [2nd heating]	°C	-*	150.5	122.9
T_m (peak) [2nd heating]	°C	342.7	341.3	339.5
Crystallization enthalpy	J/g	- 40.5	- 57.8	- 43.9
Degree of crystallinity	%	31.1	44.4	33.7
Crystallization exotherm	J/g	44.4	48.2	42.7

The value of the T_g for a heating rate of 10°C/min is the one closer to the value given in the datasheet of the material (150°C). On the other hand, melting temperature presents less variability when the heating rate is changed, around the 341°C. In this case, the value is close to the value given in the datasheet (343°C). There is also a high degree of crystallinity, higher than 30% in all cases except for the degree of crystallinity for the first heating of the sample heated at 20°C/min.

The melting temperatures obtained from the DSC would suggest that the PEEK would be able to withstand the curing temperatures of the polyimide resin with relative ease. Furthermore, the temperature needed to reach to melt the material is lower than the post-curing temperature, meaning it would be possible to melt it at a reasonable temperature to extract it from inside the composite's matrix.

4.1.2 PPS

The DSC scans for the PPS are shown in Figure A4 - Figure A6. In addition, in Figure 31 is shown the DSC test for a heating rate of 10°C/min. As happened with the PEEK results,

it can be noticed that the DSC is divided into three sections: first heating, cooling, and second heating.

In this case, it was not possible to identify the T_g peak during the first heating. It appears to be some instability in the measurement during the first minutes of the test. However, it was possible to identify the T_g on the second heating. As happened in the case of the PEEK, the T_g peak was also quite subtle. On the other hand, the melting peaks and the crystallization peak during the cooling are perfectly defined.

Table 5. *Glass transition temperature, melting temperature, crystallization enthalpy and degree of crystallinity of the PSS, extracted from the DSC curves for the three heating rates (Figure A4 - Figure A6).*

	Unit	5°C/min	10°C/min	20°C/min
Tg [1st heating]	°C	-	-	-
T_m (peak) [1st heating]	°C	276.7	277.0	277.1
Crystallization enthalpy	J/g	-24.9	-23.3	-23.8
Degree of crystallinity	%	31.1	29.1	29.8
Tg [2nd heating]	°C	93.8	92.3	97.9
T_m (peak) [2nd heating]	°C	271.2	272.5	271.7
Crystallization enthalpy	J/g	-19.4	-19.8	-21.4
Degree of crystallinity	%	24.3	24.8	26.8
Crystallization exotherm	J/g	24.1	22.9	22.1

Table 5 shows the values of T_g, T_m, crystallization enthalpy, and degree of crystallinity extracted from the DSC tests shown in Figure A4 - Figure A6. For the PPS, the values obtained are more consistent for the different heating rates than the ones obtained for the PEEK. The variation of the melting temperature for the different heating rates is lower than 1°C in each of the heating rates. Contrary to that, there is a difference of around 5°C between the melting temperature values of the first and second heating for each heating rate. These values ranged between 277.1°C and 271.2°C, which are considerably lower than the ones of the PEEK, as was expected.

The glass transition temperature was also lower than the one of the PEEK. In this case, the T_g values had less variation than the T_m values for different heating rates. However, this variation was still lower than the one observed on the PEEK values. The minimum value obtained was for the T_g obtained with a heating rate of 10°C/min, which was 92.3°C. On the other hand, the maximum value was 97.9°C obtained with a heating rate of 20°C/min. The degree of crystallinity obtained was around 30% for the first heating and around 25% for the second heating. For all three different heating rates, it is maintained that the degree of crystallinity decreases after the cooling.

The melting temperatures obtained for the PPS are around 50°C below the curing onset of the NEXIMID® MHT-R. This would suggest that the material would melt while the resin was curing. In the worst-case scenario, the material would lose its integrity before the resin was fully cured, making it impossible to achieve the desired microvascular network.

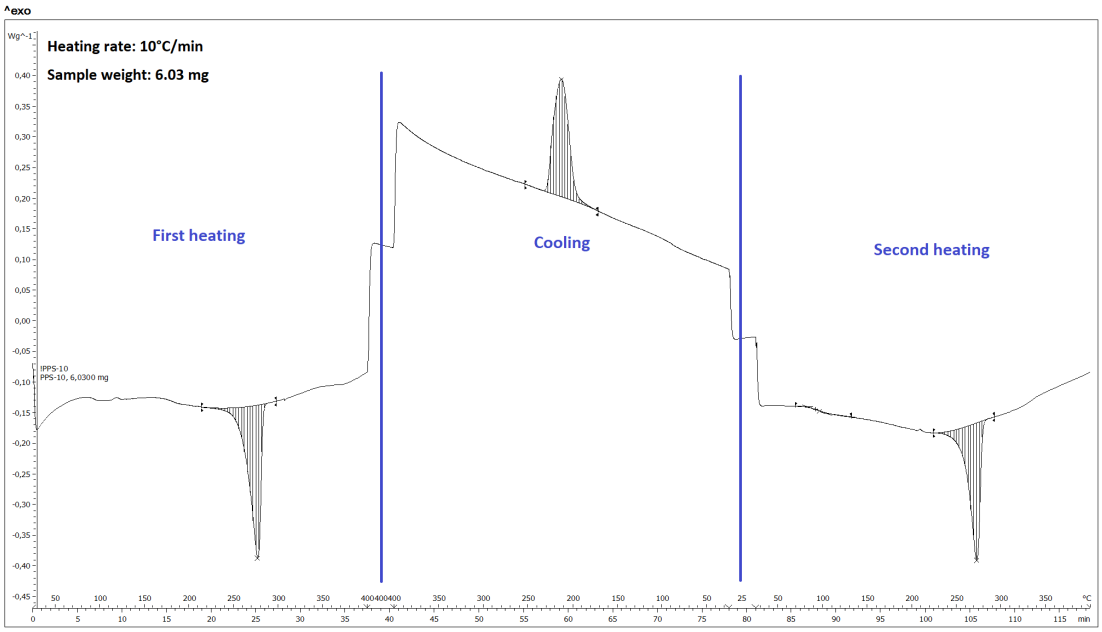

Figure 31. *DSC results for a PPS sample with a heating/cooling rate of 10°C/min. For better visualization, the same image is shown in Figure A5.*

4.1.3 PC

The DSC scans for the PC are shown in Figure A7 - Figure A9. In addition, Figure 32 shows the DSC test for a heating rate of 10°C/min. As the previous results, the test is divided into three sections. Since the PC is an amorphous thermoplastic, it does not have crystallinity. Thus, it does not present melting nor crystallization peaks. However, unlike the previous cases, the T_g presents a significant peak, making it easier to identify. In Table 6 are the values of the T_g obtained from the DSC curves. There is not a big variation of the values between the first and second heating for each heating rate. The biggest difference can be found in the test done at 20°C/min, where the T_g dropped a little bit more than 2°C compared to the first heating.

Comparing the different heating rates, it can be noticed that as the heating rate increases the T_g decreases. Taking into consideration that T_g marks the point at which the mobility of the molecule increases, it is expected that it will decrease with an increasing heating rate. If the temperature increases at a higher rate, the molecules do not have time to properly accommodate. Thus, the effect of the T_g is observed later (at higher temperatures).

Table 6. *Glass transition temperature of the PC, extracted from the DSC curves for three heating rates (Figure A7 - Figure A9).*

	Unit	5°C/min	10°C/min	20°C/min
Tg [1st heating]	°C	147.1	149.4	152.8
Tg [2nd heating]	°C	147.0	148.4	150.4
Tg [Cooling]	°C	145.4	144.8	143.1

Even though the T_g values for the PC are higher than the ones obtained for the PPS it has no crystallinity. This means that probably its fluidity will have greatly increased when reaching the curing temperatures of the polyimide resin.

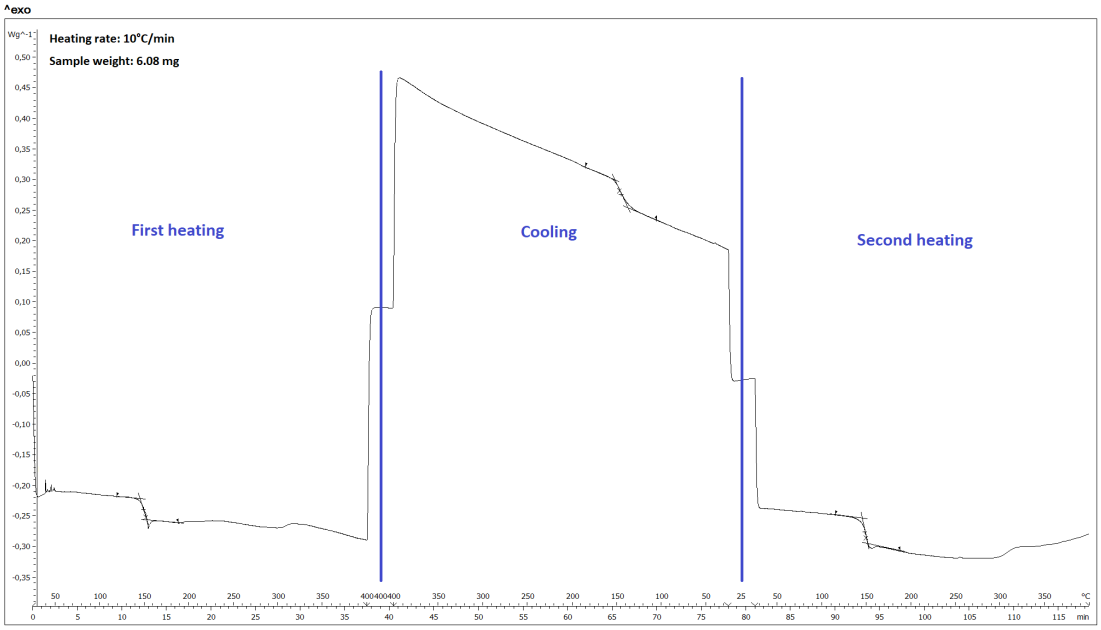

Figure 32. *DSC results for a PC sample with a heating/cooling rate of 10°C/min. For better visualization, the sample image is shown in Figure A8.*

4.2 Thermogravimetric Analysis

TGA was performed to see the degradation behavior of the different materials. Early degradation of the sacrificial material while the matrix is not cured could cause the apparition of unwanted defects beyond the empty channels. On the other hand, a high degradation of the material for higher temperatures could indicate that the material could be removed by degrading it.

The idea is to remove the sacrificial material by melting it after the matrix is cured to have empty microvascularities. However, early degradation of the sacrificial material

while the matrix is not cured could cause the apparition of unwanted defects beyond the empty channels.

As earlier explained, the TGA tests were done for each of the materials. Figure 33 shows the results of the TGA for the three different materials. It shows the weight of the sample, as a percentage, as a function of the time. The 100% weight represents the weight of the sample once it reached the desired temperature. This way, the initial weight fluctuations of the equipment and the weight loss due to moisture loss were removed from the figure. At the same time, the initial time (0 min) corresponds to the time the system reached the desired temperature.

For all three materials, the weight loss after one hour is low. In the case of the PEEK, the sample barely loses 0.2% of its weight. For the case of the PPS, this weight loss after one hour reaches 0.3%. The bigger change is found in the PC, with a loss of up to 0.6% of the initial weight. However, this is still a low value considering that it does not even reach 1%. Furthermore, it would be expected that the PC curve would show a shape like the one of the PPS and PEEK. Which would mean that even though the PC would keep losing weight with more time, the tendency of it would be to suffer a decrease in the rate at which the weight is lost.

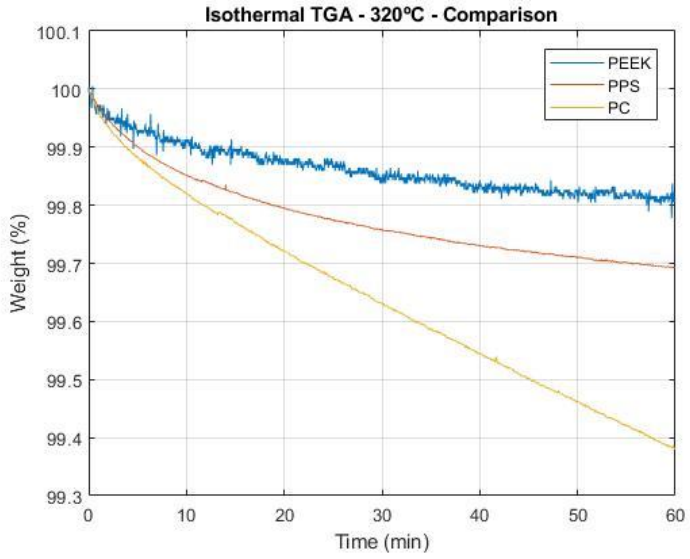

Figure 33. *Isothermal TGA of the PEEK, PPS, and PC for a time of 1h. The percentage of total weight of the sample is represented through time.*

The low weight loss shown by the different materials suggests that there is not a big degradation on the different materials at the temperature of 320°C. Thus, the liberation of gasses that could cause unwanted defects is minimum. It can be said that the three materials can withstand a curing temperature of 320°C without suffering damage that would cause a problem during the curing of the matrix. On the other hand, this good

thermal stability would indicate that it would be difficult to completely remove these materials by thermal degradation without damaging the matrix.

4.3 Small-Scale Experiments

Once the results of the DSC and TGA were obtained and it was seen that the material could be suitable for the application, the small-scale tests were done. The purpose of these tests was to see if the material could flow by itself once the melting temperature was reached.

4.3.1 PEEK

Pictures were taken before and after the test. These pictures are shown in Figure 34. The first thing that stands out is the change in the color of the sample. After the test, it got a darker color. This could have been caused by oxidation in the material. It is important to point out that the furnace test was done in an air atmosphere, not like the TGA.

Figure 34. *Close-up picture if of the PEEK samples before and after the test. a) Sample before the test. It has some sharper angles and square-shape section. Its color is clear. b) Sample after the test. It has lost its angles. Round-like section. It has become darker.*

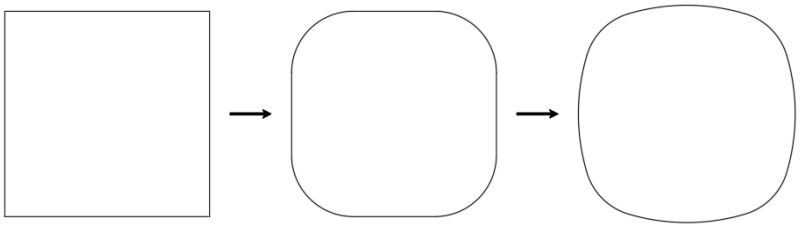

Figure 35. *Schematic image of the change of the chape in the PEEK samples after the test. The samples that previously had a square-shaped section loses the sharp edges into a more circular section.*

It is also appreciable that before the test, the sample presents a sharper shape, with angles on the edges, giving a square-shaped section. Once the test was done, the sample presented a more round-like shape. Figure 35 shows a schematic illustration of this change. The squared shape loses the angles and turns into a rounder shape. However, it is still possible to guess the previous squared shape that the sample had before the test.

Finally, Figure 36 shows a picture of the sample with a squared pattern on the background as a reference for the size. Each square is 5 mm x 5 mm. The sample suffered a shrinkage in its longitudinal direction. The length of the sample before the test was around 45 mm, while after the test the length of the sample was around 42mm. This means the sample suffered shrinkage of 6.7% on its longitudinal direction. It might be shrinkage also in the transversal direction of the sample, but the change of shape and color, and the low thickness make it difficult to notice. The results suggest that even though the material passed to a melt state, it cannot flow by itself. The sample thickness has lower than the tube's inner diameter. This means that if the material would have flowed, gravity would have pulled it to the bottom of the tube. If that would have happened it would have been seen a major reduction in the sample length, which would also have increased its thickness to fill the space inside the tube.

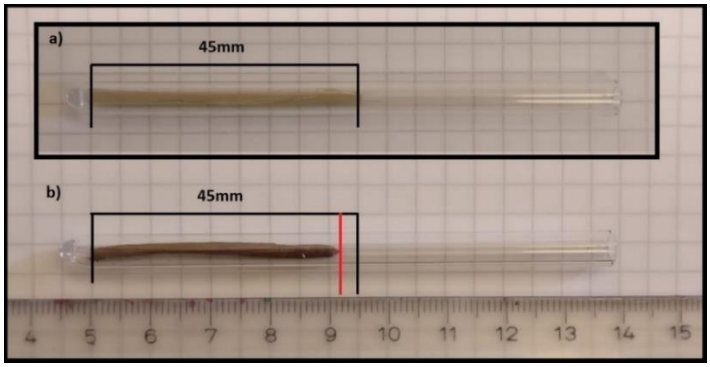

Figure 36. *PEEK sample before and after the test. Each square is 5x5 mm for reference. a) Sample before the test. b) Sample at the end of the test.*

4.3.2 PPS

It was expected that with lower thermal stability the melt would have less viscosity at the required temperatures. The scale tests were repeated with PPS samples. Figure 37 shows a picture of the sample before and after the test. The behavior shown by the PPS was highly similar to the one observed in the PEEK. As happened with the PEEK there is an appreciable change of color in the sample. In this case, the change is more subtle since the material has already dark color. But it is possible to see that it went from a dark brown color to almost black.

Another similarity appreciable in both cases is the change in the shape of the piece. Although it is still possible to see some edges on the sample after the test, these are less sharp than before. However, as happened with the PEEK, it is still clear that even though the material reached a melt state, it could not flow by itself inside the tube. It is still possible to see that the material did not fill the bottom part of the tube, which would have happened if the material had turned liquid enough. Also, once again the sample suffered a reduction in length. In this case, the longitudinal shrinkage was around 2%.

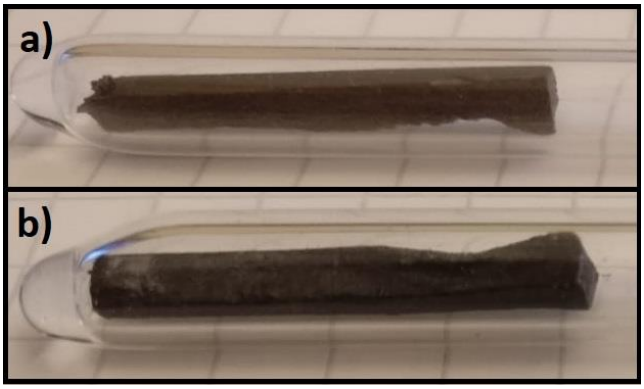

Figure 37. *Close-up picture of the PPS samples before and after the test. a) Sample before the tests. It has sharper angles and square shaped section. It also is slightly clearer in color. b) Sample after the test. It lost its angles, now having a round-like section. Darker color.*

4.3.3 PC

Finally, the PC was tested using the same procedure used for the other two materials but with an even lower temperature than the PPS. PC was the material with the lower thermal stability of the three. Figure 38 shows the PC samples used in the test. First of all, Figure 38a and Figure 38b show a piece of PC that was placed in a petri dish.

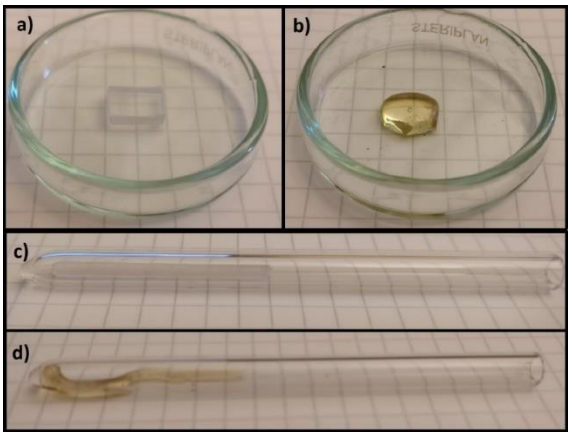

Figure 38. *Close-up pictures of the PC samples before and after the test. a) PC piece on a petri dish before the test. b) Same PC piece after the test. c) Sample on the tube before the test. d) Same sample inside the tube after the test.*

Once again, as happened with the previous two materials, it can be seen a change in the color of the material, which got a yellowish color. However, what outstands, in this case, is the change in the geometry. In this case, a completely round droplet was formed, which means that this material reached a liquid state.

4.4 Scale model test

The scale model test was a more accurate simulation made to ensure that there was no interaction between the NEXIMID® MHT-R polyimide resin and the different tested materials. A reaction between matrix and sacrificial material would not allow easy removal of the latest. An optical microscope was used to see the point where the two materials met.

4.4.1 PEEK

The two PEEK samples were observed, one with resin that had only been melted at 250°C (Figure 39) and one with resin that was firstly melted at 250°C and then cured for 1 hour at 340°C (Figure 40). In both cases, the whiter zone is the PEEK sample while the darker zone is the polyimide resin. It is appreciable a perfect division between the two materials. The interface between these two is well defined and does not appear that the PEEK has dissolved into the polyimide resin in any of the two cases.

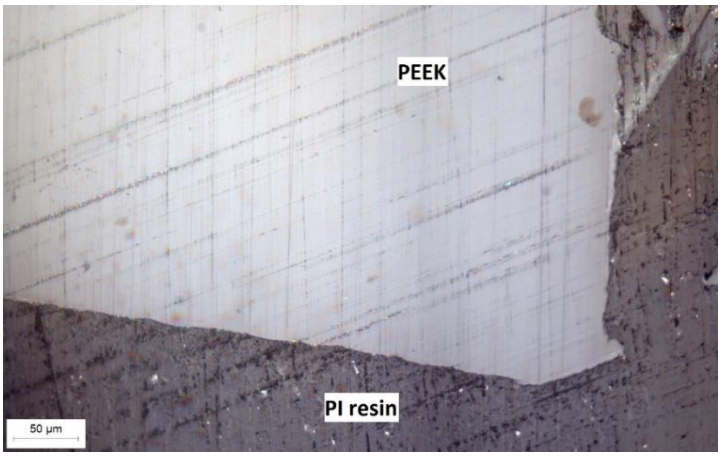

Figure 39. *Microscope image from a contact point between a PEEK sample and the NEXIMID® MHT-R that had been melted at 250°C.*

In Figure 39 it is also possible to identify a change in the color of the resin in the upper right corner of the image. This has been attributed to the fact that during the experimental procedure resin powder was introduced into the tube and melted twice.

Probably the change in the color is because the two sections belong to the two different batches.

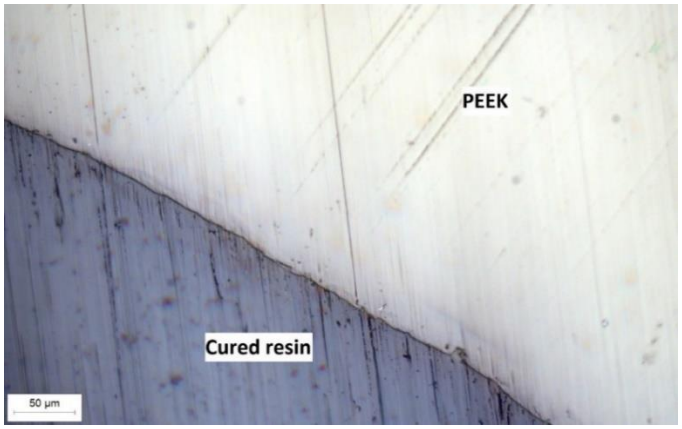

Figure 40. *Microscope image from a contact point between a PEEK sample and the NEXIMID® MHT-R that had been cured at 340°C for 1hour.*

4.4.2 PPS

Only one PPS sample was embedded into resin powder. Unexpectedly, as can be seen in Figure 41, the PPS sample appeared to have a reinforcement, probably glass fiber. The material was thought to be just PPS polymer, so at first, it was thought that this was caused by some interaction with the resin. However, the filler was too evenly distributed around the PPS. To get out of doubt, a sample of just the PPS material (without resin) was mounted for microscope observation. Figure 42 corresponds to this sample. As can be seen, the PPS sample presents the dotted pattern that indicates that it has a filler, which ensures that it had nothing to do with the resin.

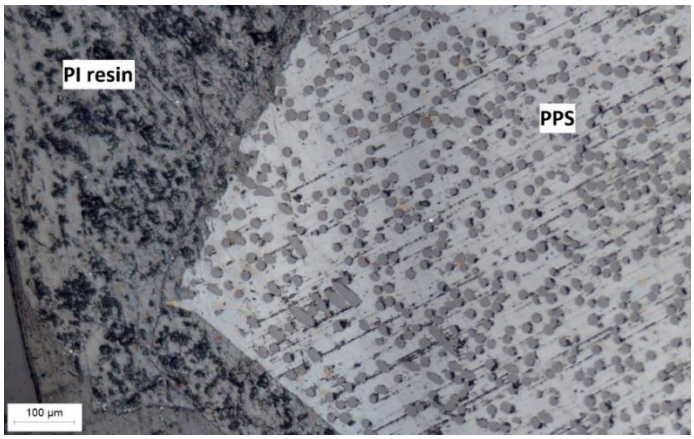

Figure 41. *Microscope image from a contact point between a PPS sample and the NEXIMID® MHT-R that had been melted at 250°C.*

As happened with the PEEK, the interface between the PPS and the resin is well defined, and seems that the PPS has not dissolved into the resin. However, discovering that the PPS material was reinforced with glass fiber would invalidate the small-scale test done to see the flowability of the material, since the presence of these fibers produces an increase in viscosity, preventing the flow of the material.

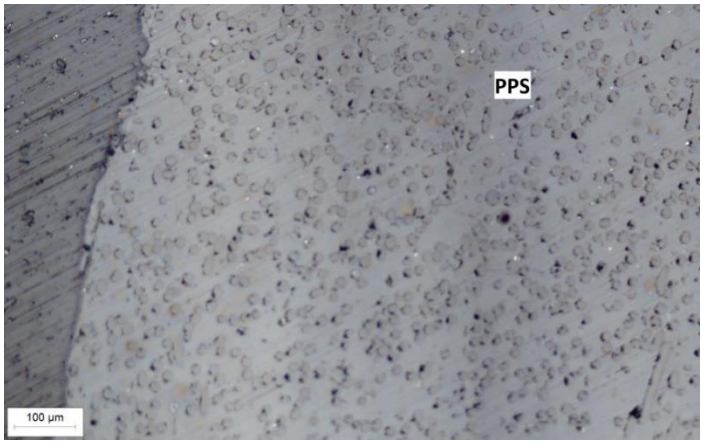

Figure 42. *Microscope image from a PPS sample, without polyimide resin.*

4.4.3 PC

The result of the PC sample is shown in Figure 43. Once again it is easy to identify the line between the PC and the polyimide resin. There is a good separation between the two materials and looks like the PC did not dissolve into the polyimide. However, it must be pointed out that the shape of the polycarbonate is completely lost. The sample used for the test was a prism with a squared section sized around 1 x 1 x 40 mm.

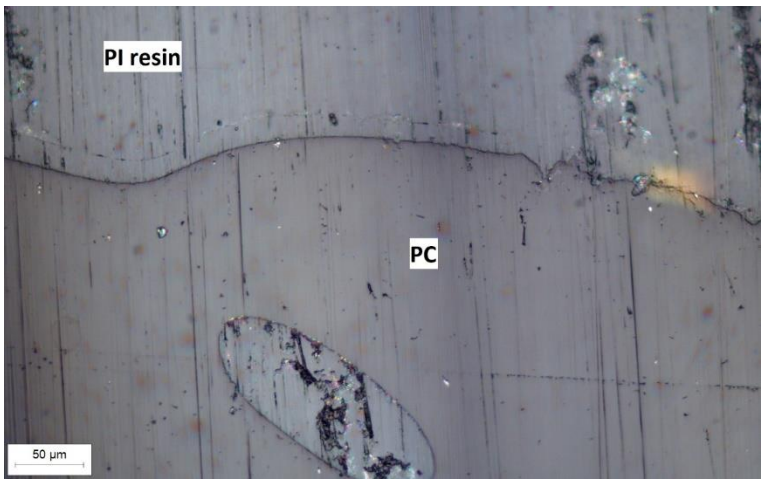

Figure 43. *Microscope image from a contact point between a PC sample and the NEXIMID® MHT-R that had been melted at 250°C.*

Figure 44 shows the same sample with fewer magnifications. Here it is easier to see how the PC lost the prismatic shape and passed to a fluid state. It is possible to see how the PC and the resin formed a heterogenic mixture inside the tube. This loss of shape of the PC happened at 250°C, which is way lower than the curing temperature of the resin.

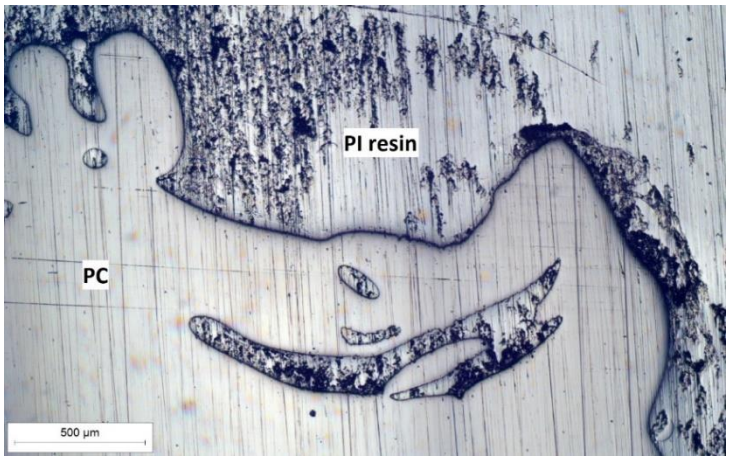

Figure 44. *Same sample as shown in Figure 43 with lower magnification.*

5. CONCLUSIONS

Different tests were performed to evaluate the properties and behavior of the different materials to analyze their viability as sacrificial materials. DSC was performed to see the thermal physical changes of the materials. TGA was done to see the degradation suffered by the different materials at the curing temperature of the polyimide resin. A small-scale test was performed to see the flowability of the different materials in an environment that simulates the composite manufacturing conditions. Scale model test was done to ensure that the different candidates did not dissolve into the polyimide resin.

The PEEK presented thermal stability enough to withstand the curing temperatures and did not dissolve into the polyimide. The DSC results showed a melting temperature that suggested it would be a good choice. However, the small-scale test showed that even though the melting temperature was greatly surpassed, there was no fluidization of the material. For these reasons, although it presented ideal thermal stability, this same stability is the one that would not make it possible to remove the PEEK from inside the composite by simply melting it. There is no straightforward way to use the studied PEEK as a sacrificial material. It appears that it would be easy to place it in the composite and it would withstand all the curing process, but it would be no simple way to remove it after that.

The PPS presented a behavior similar to the one of the PEEK. It had good thermal stability at curing temperatures and did not dissolve into the resin. Also, despite surpassing the melting temperature, no spontaneous flow was registered in the small-scale test. The results for PPS are very preliminary since the scale model test revealed that the material used was a fiber-reinforced composite grade. Thus, even though the samples tested did not exhibit the features set necessary for the application, it is necessary to bear in mind that it was reinforced, and it was not pure PPS.

The PC behavior was the opposite of the one seen in the other two materials. It also had good thermal stability shown by the TGA. In addition, it appeared not to dissolve into the polyimide. However, the PC passed to a liquid-like state already visible at 250°C, which was way lower than the curing temperatures of the chosen polyimide resin. Thus, although this would allow easy removal by just melting the material, it has been considered not viable to use. The microvascular network would lose all its shape with such early fluidization of the material.

6. FUTURE WORK

Different considerations have been considered regarding possible future work after the one done in this thesis:

The PEEK degree used for this project was the VICTREX® 450G. There is another degree, VICTREX® 90G, which the technical datasheet says has a viscosity at 400°C more than three times lower than the one of the 450G. Maybe the degree used was especially viscous, which made it more difficult for the material to flow. Testing lower viscosity degrees would be a good start.

There is also the possibility of using blends, copolymers, or additives that would allow the fluidization of the material at lower temperatures. An example of this is the one used in the VaSC technique, where PLA is blended with tin oxalate to reduce the vaporization temperature of the PLA to 200°C [1][23]. Since the PEEK material is known and outstands for its good thermal properties, it is unlikely that exist previous studies that would try to decrease this thermal stability. It would be interesting to explore.

One simpler possibility is the exploration of different materials. In this project, three materials have been tested and one resulted to have a filling material. Trying out PPS material without fillings could be a good start. Several high-temperature polymers could be tested. Some options could be other PAEKs, PTFE, or PA46. DSC results obtained in this project could be useful to relate the properties of the material with the behavior observed in the small-scale test.

The use of DMTA tests could be useful when exploring new materials. The evaluation of the softening point before further tests could save time and allow a first screening of the options.

7. BIBLIOGRAPHY

[1] S. J. Pety, M. H. Y. Tan, A. R. Najafi, P. R. Barnett, P. H. Geubelle, and S. R. White, "Carbon fiber composites with 2D microvascular networks for battery cooling," *Int. J. Heat Mass Transf.*, vol. 115, pp. 513–522, 2017, doi: 10.1016/j.ijheatmasstransfer.2017.07.047.

[2] M. U. Saeed, Z. F. Chen, and B. Bin Li, "Manufacturing strategies for microvascular polymeric composites: A review," *Compos. Part A Appl. Sci. Manuf.*, vol. 78, pp. 327–340, 2015, doi: 10.1016/j.compositesa.2015.08.028.

[3] C. M. Dry and N. R. Sottos, "Passive smart self-repair in polyme matrix composites," *Smart Struct. Mater. 1993 Smart Mater.*, vol. 1916, no. July 1993, pp. 438–444, 1993, doi: 10.1117/12.148501.

[4] C. Dry, "Procedures developed for self-repair of polymer matrix composite materials," *Compos. Struct.*, vol. 35, no. 3, pp. 263–269, 1996, doi: 10.1016/0263-8223(96)00033-5.

[5] M. Motuku, U. K. Vaidya, and G. M. Janowski, "Parametric studies on self-repairing approaches for resin infused composites subjected to low velocity impact," *Smart Mater. Struct.*, vol. 8, no. 5, pp. 623–638, 1999, doi: 10.1088/0964-1726/8/5/313.

[6] D. Roach, "Real time crack detection using mountable Comparative Vacuum monitoring sensors," *Smart Struct. Syst.*, vol. 5, no. 4, pp. 317–328, 2009, doi: 10.12989/sss.2009.5.4.317.

[7] J. G. Hemrick, E. Lara-Curzio, E. R. Loveland, K. W. Sharp, and R. Schartow, "Woven graphite fiber structures for use in ultra-light weight heat exchangers," *Carbon N. Y.*, vol. 49, no. 14, pp. 4820–4829, 2011, doi: 10.1016/j.carbon.2011.06.094.

[8] D. M. Phillips, M. Ryan Pierce, and J. W. Baur, "Mechanical and thermal analysis of microvascular networks in structural composite panels," *Compos. Part A Appl. Sci. Manuf.*, vol. 42, no. 11, pp. 1609–1619, 2011, doi: 10.1016/j.compositesa.2011.07.008.

[9] A. R. Hamilton, N. R. Sottos, and S. R. White, "Local strain concentrations in a microvascular network," *Proc. Soc. Exp. Mech. Inc.*, vol. 67, no. September 2009, pp. 255–263, 2010, doi: 10.1007/s11340-009-9299-5.

[10] A. R. Hamilton, N. R. Sottos, and S. R. White, "Pressurized vascular systems for self-healing materials," *J. R. Soc. Interface*, vol. 9, no. 70, pp. 1020–1028, 2012, doi: 10.1098/rsif.2011.0508.

[11] A. S. Wu *et al.*, "Sensing of damage and healing in three-dimensional braided composites with vascular channels," *Compos. Sci. Technol.*, vol. 72, no. 13, pp. 1618–1626, 2012, doi: 10.1016/j.compscitech.2012.06.012.

[12] R. S. Trask and I. P. Bond, “Bioinspired engineering study of Plantae vascules for self-healing composite structures,” *J. R. Soc. Interface*, vol. 7, no. 47, pp. 921–931, 2010, doi: 10.1098/rsif.2009.0420.

[13] C. J. Norris, G. J. Meadway, M. J. O’Sullivan, I. P. Bond, and R. S. Trask, “Self-healing fibre reinforced composites via a bioinspired vasculature,” *Adv. Funct. Mater.*, vol. 21, no. 19, pp. 3624–3633, 2011, doi: 10.1002/adfm.201101100.

[14] C. J. Norris, I. P. Bond, and R. S. Trask, “The role of embedded bioinspired vasculature on damage formation in self-healing carbon fibre reinforced composites,” *Compos. Part A Appl. Sci. Manuf.*, vol. 42, no. 6, pp. 639–648, 2011, doi: 10.1016/j.compositesa.2011.02.003.

[15] M. S. F. Lima, J. M. S. Sakamoto, J. G. A. Simoes, and R. Riva, “Laser processing of carbon fiber reinforced polymer composite for optical fiber guidelines,” *Phys. Procedia*, vol. 41, pp. 572–580, 2013, doi: 10.1016/j.phpro.2013.03.118.

[16] J. A. Lewis, “Direct ink writing of 3D functional materials,” *Adv. Funct. Mater.*, vol. 16, no. 17, pp. 2193–2204, 2006, doi: 10.1002/adfm.200600434.

[17] D. Therriault, R. F. Shepherd, S. R. White, and J. A. Lewis, “Fugitive inks for direct-write assembly of three-dimensional microvascular networks,” *Adv. Mater.*, vol. 17, no. 4, pp. 395–399, 2005, doi: 10.1002/adma.200400481.

[18] K. S. Toohey, “Microvascular networks for continuous self-healing materials,” *Univ. Illinois Urbana-Champaign*, 2007.

[19] K. S. Toohey, C. J. Hansen, J. A. Lewis, S. R. White, and N. R. Sottos, “Delivery of two-part self-healing chemistry via microvascular networks,” *Adv. Funct. Mater.*, vol. 19, no. 9, pp. 1399–1405, 2009, doi: 10.1002/adfm.200801824.

[20] B. D. Kozola, L. A. Shipton, V. K. Natrajan, K. T. Christensen, and S. R. White, “Characterization of active cooling and flow distribution in microvascular polymers,” *J. Intell. Mater. Syst. Struct.*, vol. 21, no. 12, pp. 1147–1156, 2010, doi: 10.1177/1045389X10379662.

[21] J. H. Huang *et al.*, “Rapid fabrication of bio-inspired 3D microfluidic vascular networks,” *Adv. Mater.*, vol. 21, no. 35, pp. 3567–3571, 2009, doi: 10.1002/adma.200900584.

[22] A. P. Esser-Kahn *et al.*, “Three-dimensional microvascular fiber-reinforced composites,” *Adv. Mater.*, vol. 23, no. 32, pp. 3654–3658, 2011, doi: 10.1002/adma.201100933.

[23] S. J. Pety, “Microvascular composites as a multifunctional material for electric vehicles,” University of Illinois, 2017.

[24] Huntsman Corporation, “Araldite ® LY8605 / Aradur® 8605 System.” 2010.

[25] P. Fernberg, G. Gong, P. Mannberg, and S. Tsampas, “Development of novel high

Tg polyimide-based composites. Part I: RTM processing properties," *J. Compos. Mater.*, vol. 52, no. 2, pp. 253–260, 2018, doi: 10.1177/0021998317705705.

[26] F. Masari, "Manufacturing induced shape distortions : high temperature thermoset composites."

[27] E. N. Peters and R. K. Arisman, "Engineering Thermoplastics," *Appl. Polym. Sci. 21st Century*, pp. 177–196, 2000, doi: 10.1016/b978-008043417-9/50012-x.

[28] D. Kemmish, *Update on the Technology and Applications of Polyaryletherketones*. 2010.

[29] D. V. Rosato, D. V. Rosato, and M. V. Rosato, *Plastic Product Material and Process Selection Handbook*, no. September. 2004.

[30] S. Ebnesajjad, "Polytetrafluoroethylene: Properties and Structure," in *Expanded PTFE Applications Handbook*, 2017, pp. 9–24.

[31] G. Wypych, *Handbook of Polymers*. Toronto: ChemTec Publishing, 2012.

[32] J. Yang, T. Xu, A. Lu, Q. Zhang, H. Tan, and Q. Fu, "Preparation and properties of poly (p-phenylene sulfide)/multiwall carbon nanotube composites obtained by melt compounding," *Compos. Sci. Technol.*, vol. 69, no. 2, pp. 147–153, 2009, doi: 10.1016/j.compscitech.2008.08.030.

[33] V. R. Sastri, *High-Temperature Engineering Thermoplastics*. 2014.

[34] S. Ebnesajjad and R. A. Morgan, *Fluorinated Additives for Plastics*. 2012.

[35] V. García Ibarra, R. Sendón, and A. Rodríguez-Bernaldo De Quirós, *Antimicrobial Food Packaging Based on Biodegradable Materials*, no. Figure 1. Elsevier Inc., 2016.

[36] G. L. Robertson, "Food Packaging," *Encycl. Agric. Food Syst.*, vol. 3, pp. 232–249, 2014, doi: 10.1016/B978-0-444-52512-3.00063-2.

[37] R. Wehrmann, "Polycarbonate," in *Encyclopedia of Materials: Science and Technology*, no. 1, 2001, pp. 7149–7151.

[38] K. Takeuchi, "Polycarbonates," *Polym. Sci. A Compr. Ref. 10 Vol. Set*, vol. 5, pp. 363–376, 2012, doi: 10.1016/B978-0-444-53349-4.00148-5.

[39] N. Niessner and H. Gausepohl, "Polystyrene and Styrene Copolymers," in *Encyclopedia of Materials: Science and Technology*, 2001, pp. 7735–7741.

[40] E. A. Growney Kalaf, K. R. Hixon, P. U. Kadakia, A. J. Dunn, and S. A. Sell, *Electrospun biomaterials for dermal regeneration*. Elsevier Ltd., 2017.

[41] S. T. Peters, "HANDBOOK OF COMPOSITES," *ASM Int.*, p. 1201, 2001.

[42] M. T. Aronhime and J. K. Gillham, "Time-Temperature-Transformation (TTT) Cure

Diagram of Thermosetting Polymeric Systems.," *Adv. Polym. Sci.*, vol. 78, pp. 83–113, 1986, doi: 10.1007/bfb0035358.

[43] M. K. Buragohain, *Composite Structures. Design, Mechanics, Analysis, Manufacturing, and Testing*. CRC Press, 2017.

8. APPENDIX

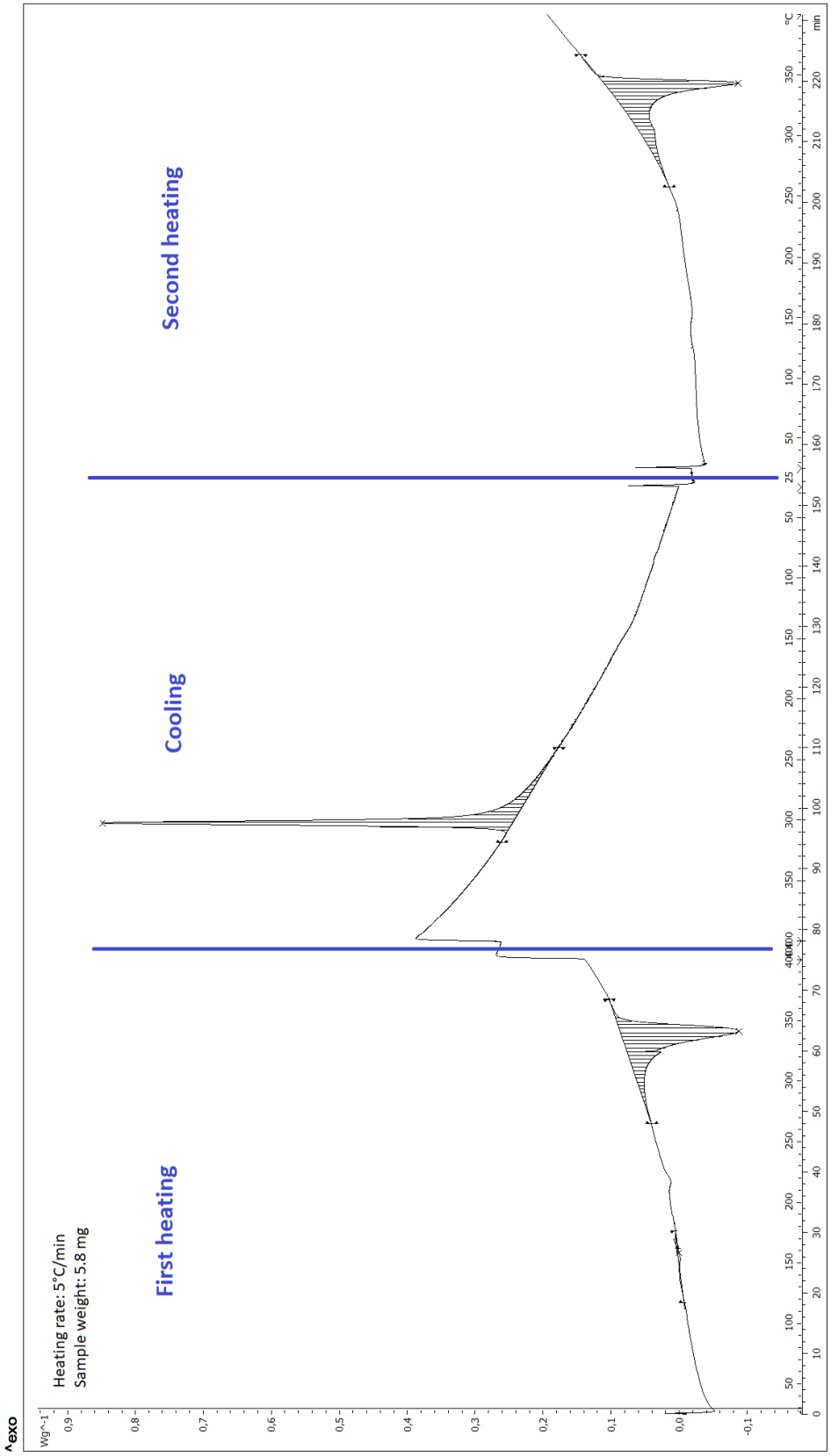

Figure A1. *DSC results for a PEEK sample with a heating/cooling rate of 5°C/min. First heating up to 400°C. Cooling down to 25°C. Second heating up to 400°C.*

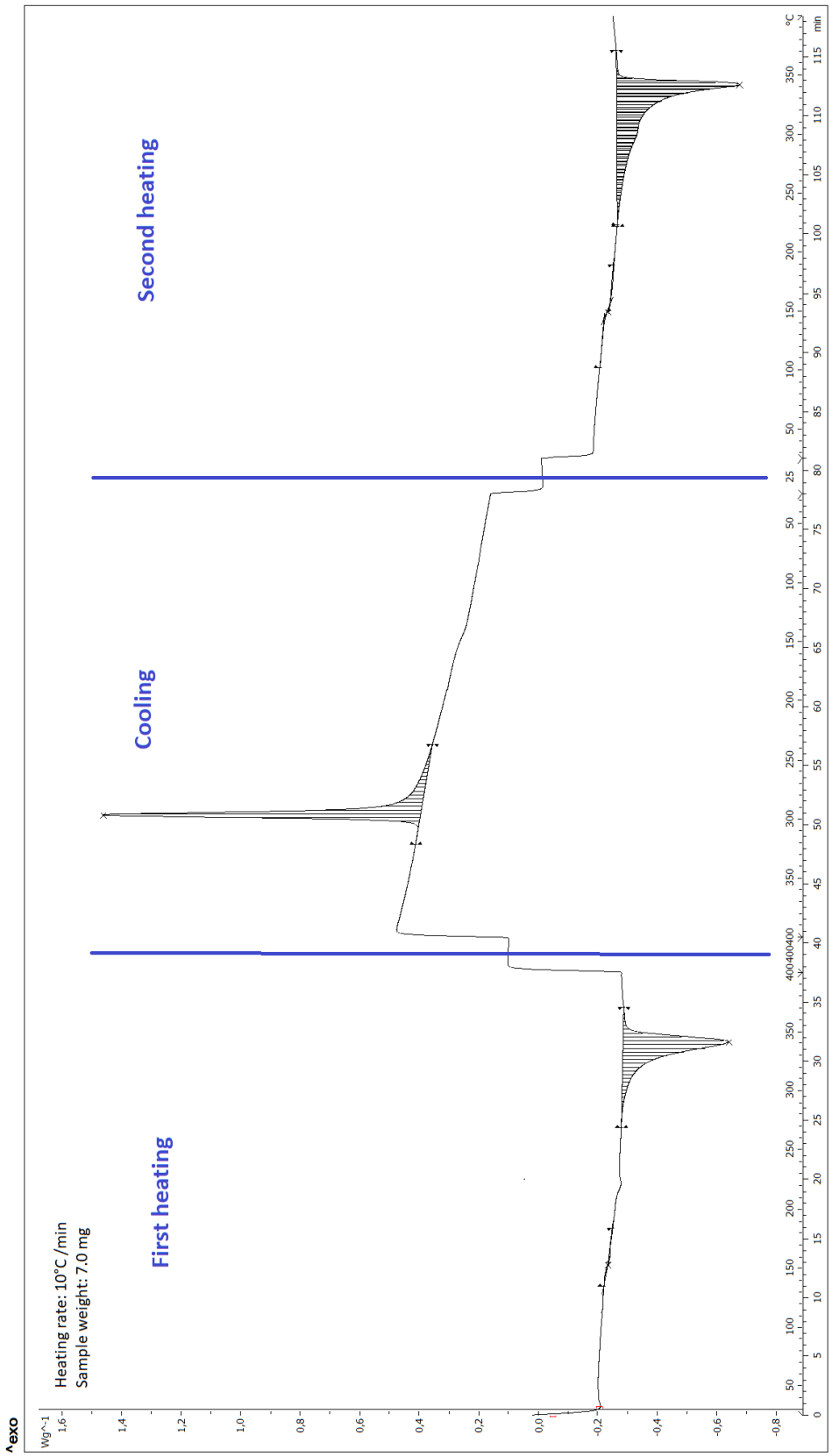

Figure A2. *DSC results for a PEEK sample with a heating/cooling rate of 10°C/min. First heating up to 400°C. Cooling down to 25°C. Second heating up to 400°C.*

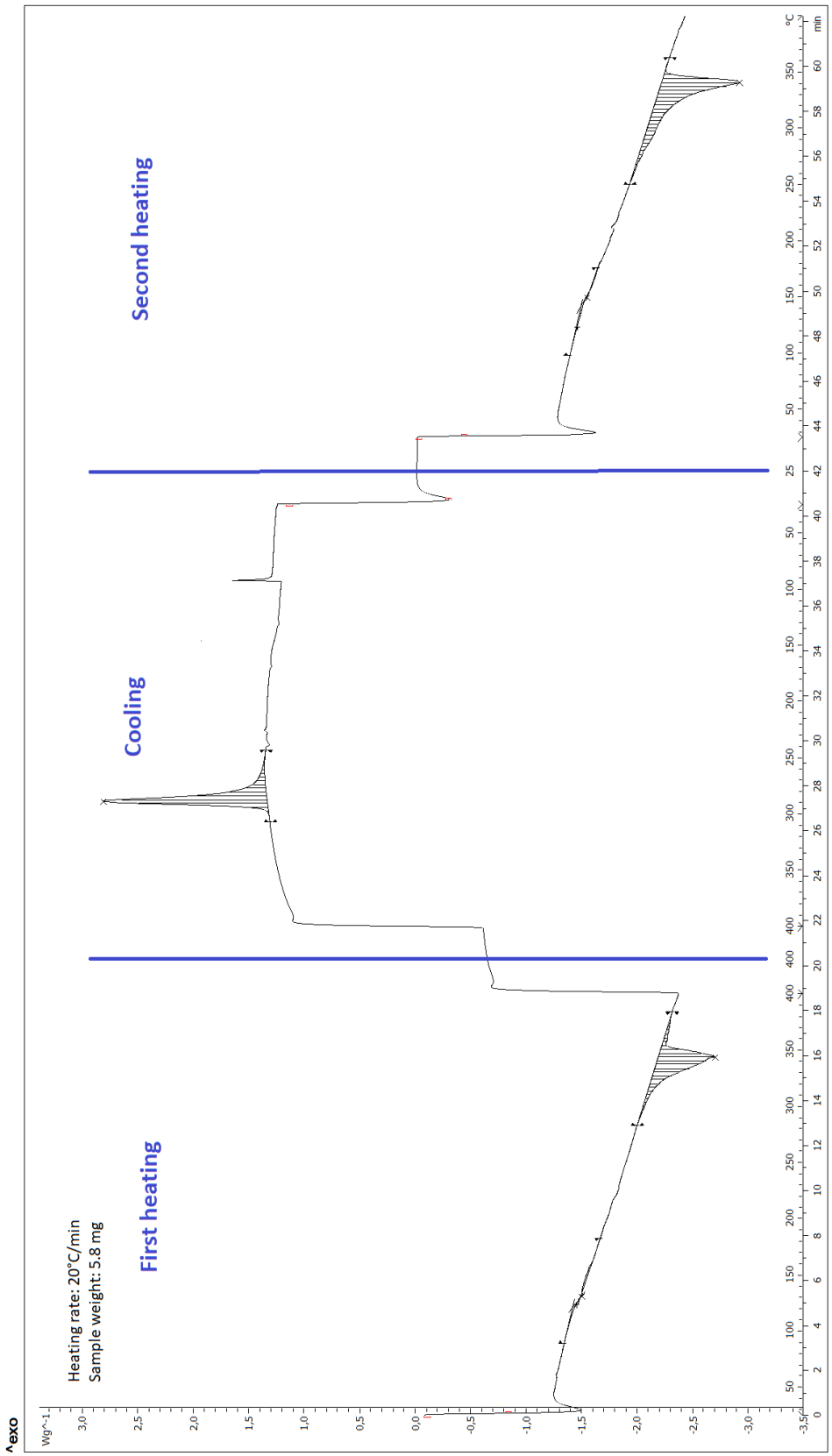

Figure A3. DSC results for a PEEK sample with a heating/cooling rate of 20°C/min. First heating up to 400°C. Cooling down to 25°C. Second heating up to 400°C.

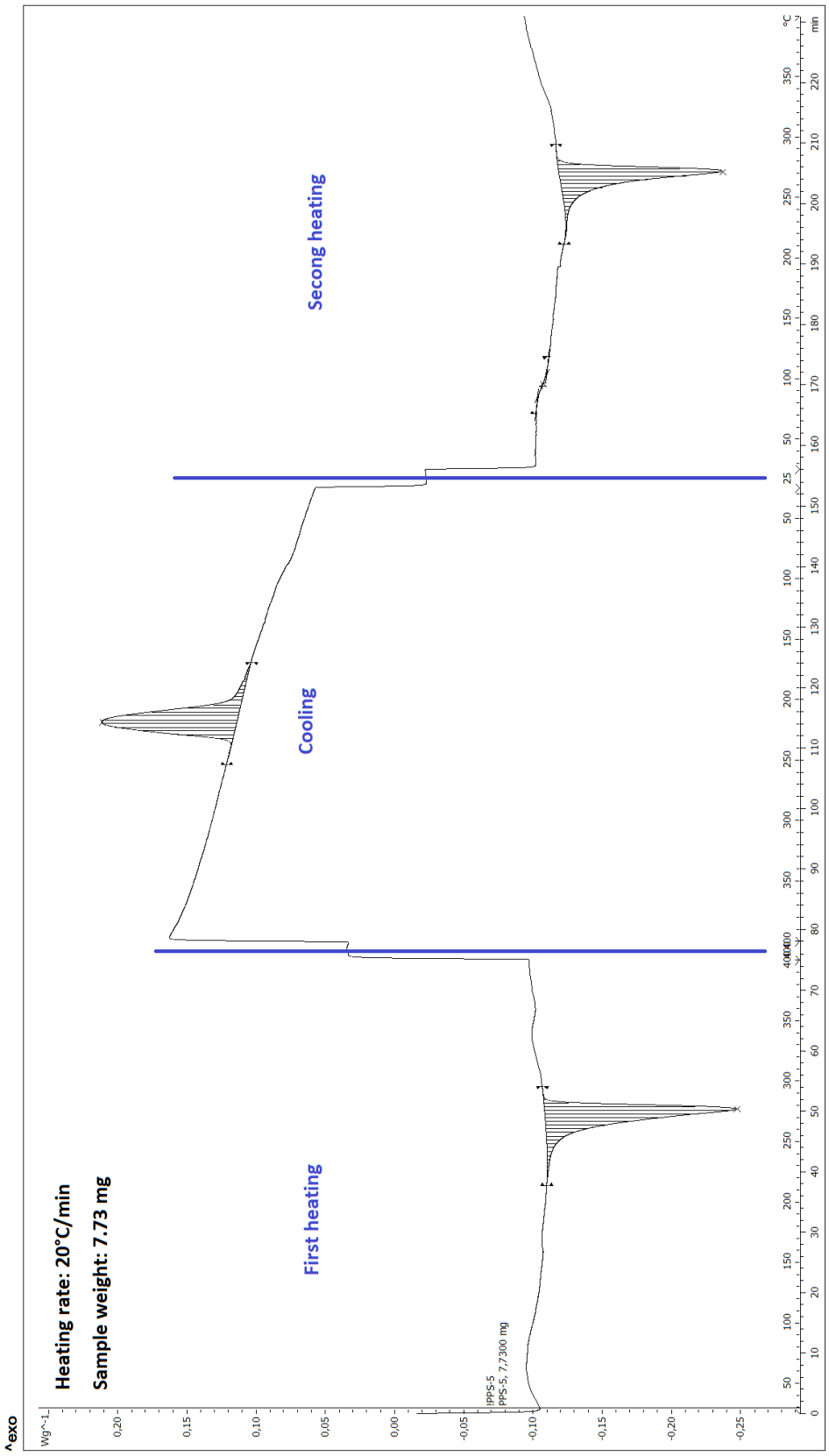

Figure A4. DSC results for a PPS sample with a heating/cooling rate of 5°C/min. First heating up to 400°C. Cooling down to 25°C. Second heating up to 400°C.

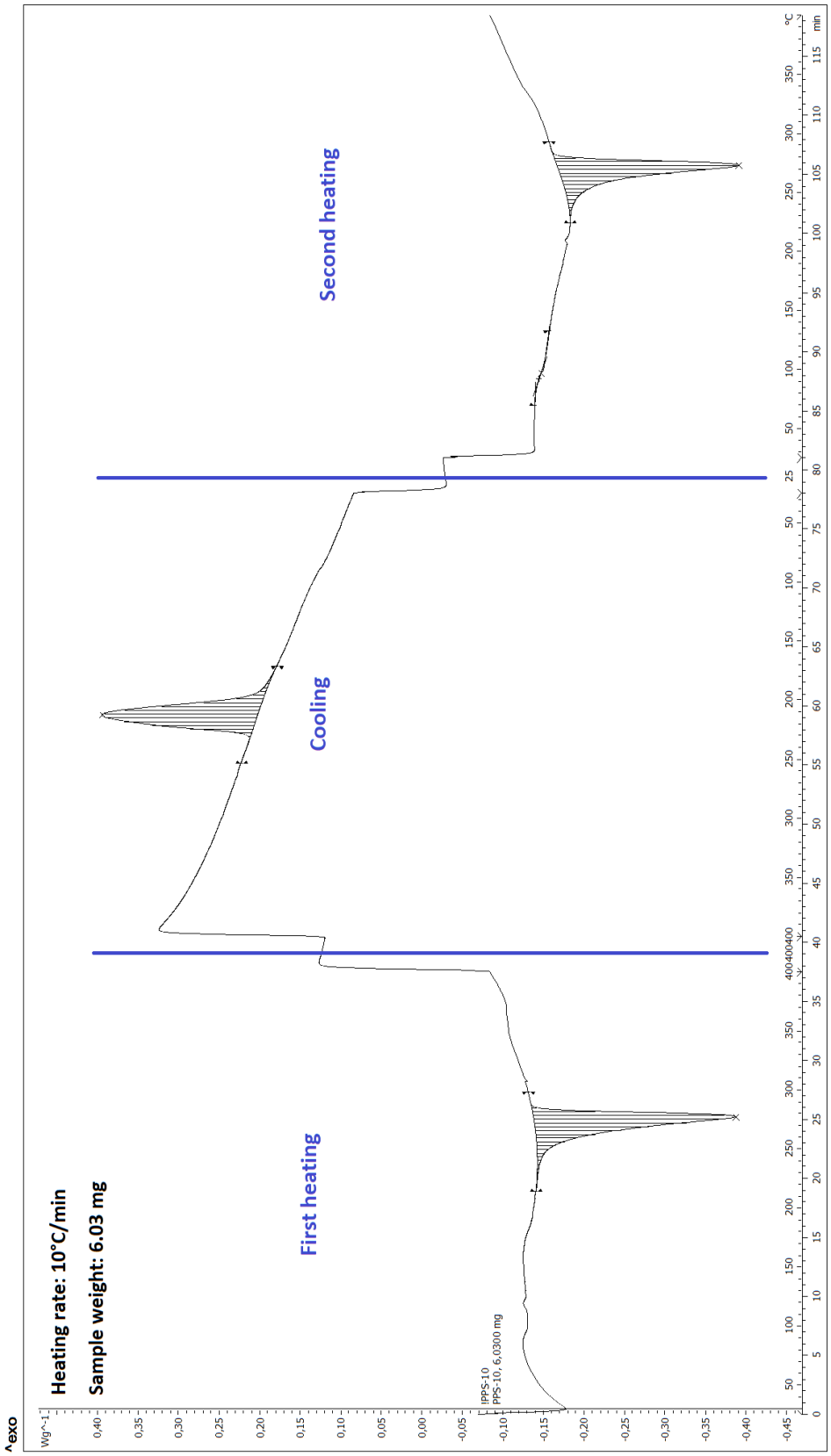

Figure A5. DSC results for a PPS sample with a heating/cooling rate of 10°C/min. First heating up to 400°C. Cooling down to 25°C. Second heating up to 400°C.

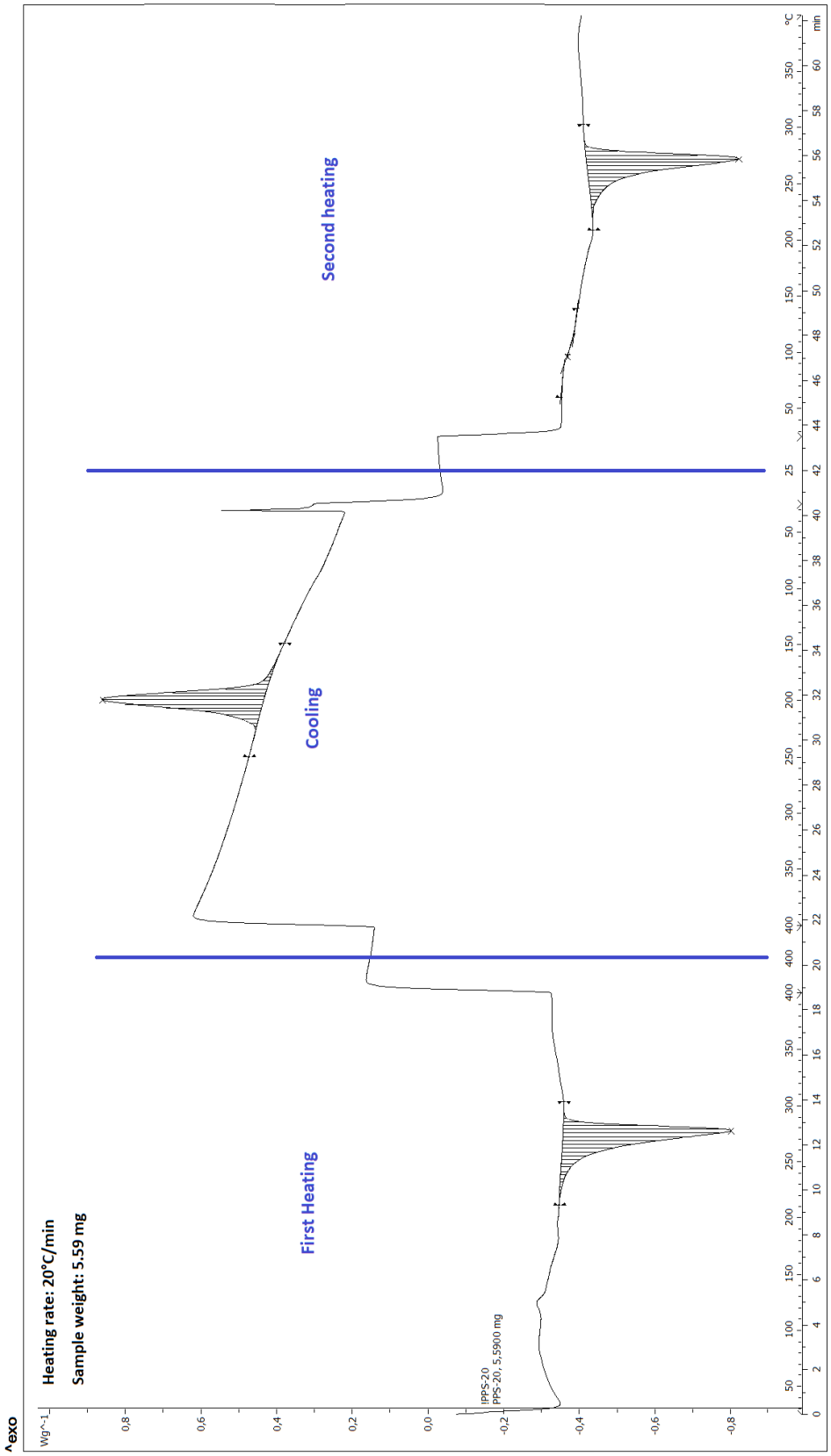

Figure A6. DSC results for a PPS sample with a heating/cooling rate of 20°C/min. First heating up to 400°C. Cooling down to 25°C. Second heating up to 400°C.

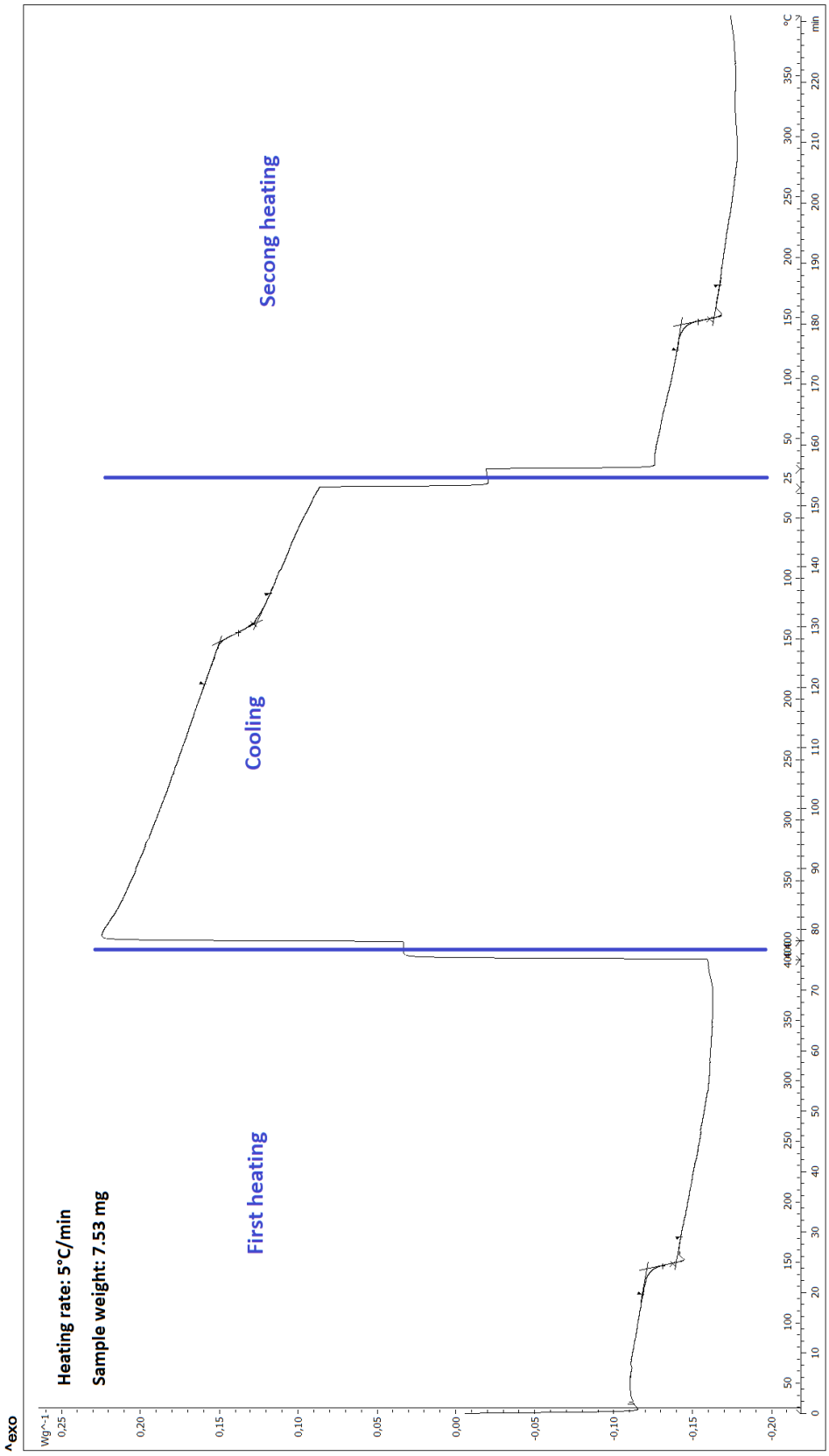

Figure A7. DSC results for a PC sample with a heating/cooling rate of 5°C/min. First heating up to 400°C. Cooling down to 25°C. Second heating up to 400°C.

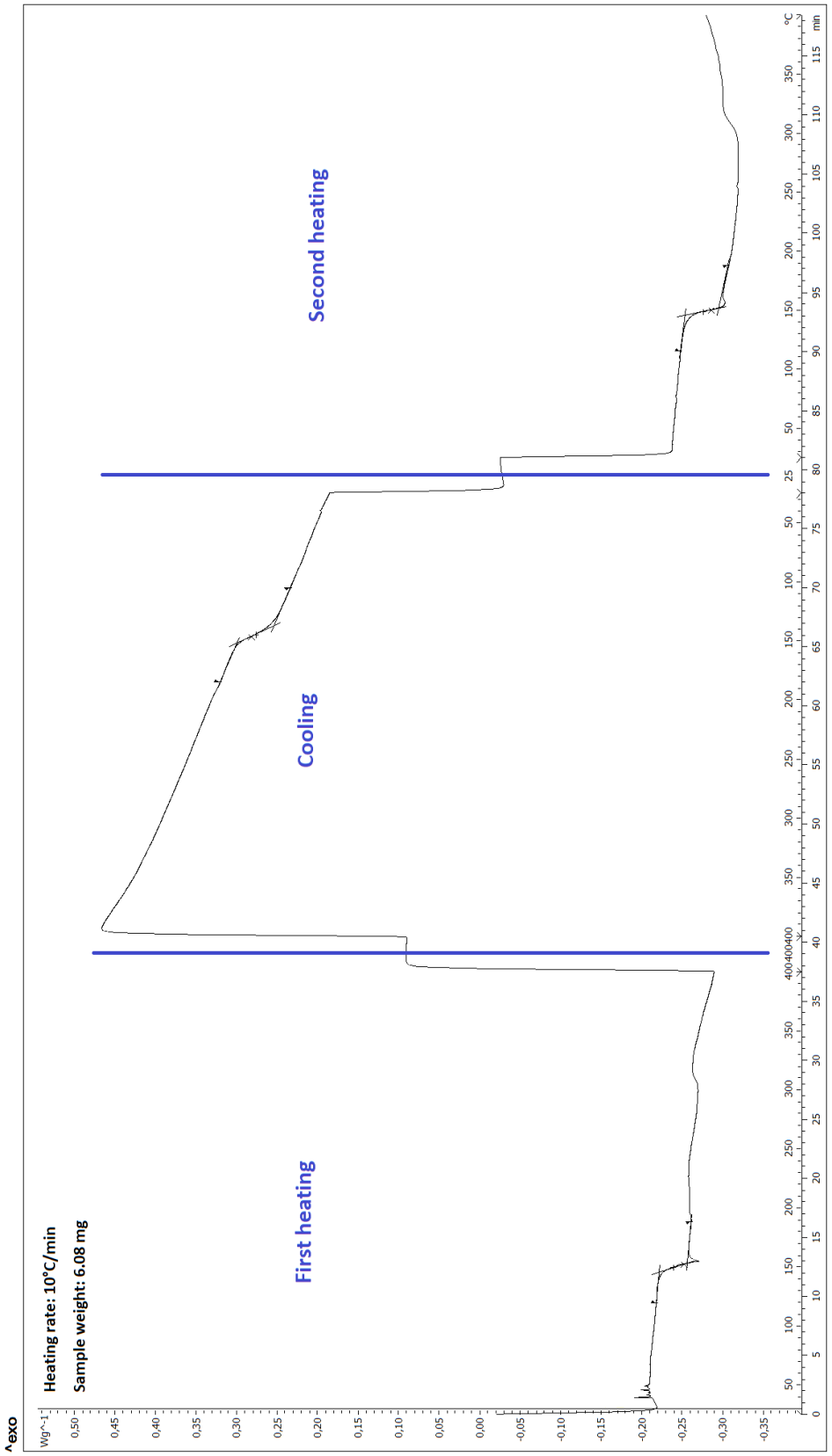

Figure A8. DSC results for a PC sample with a heating/cooling rate of 10°C/min. First heating up to 400°C. Cooling down to 25°C. Second heating up to 400°C.

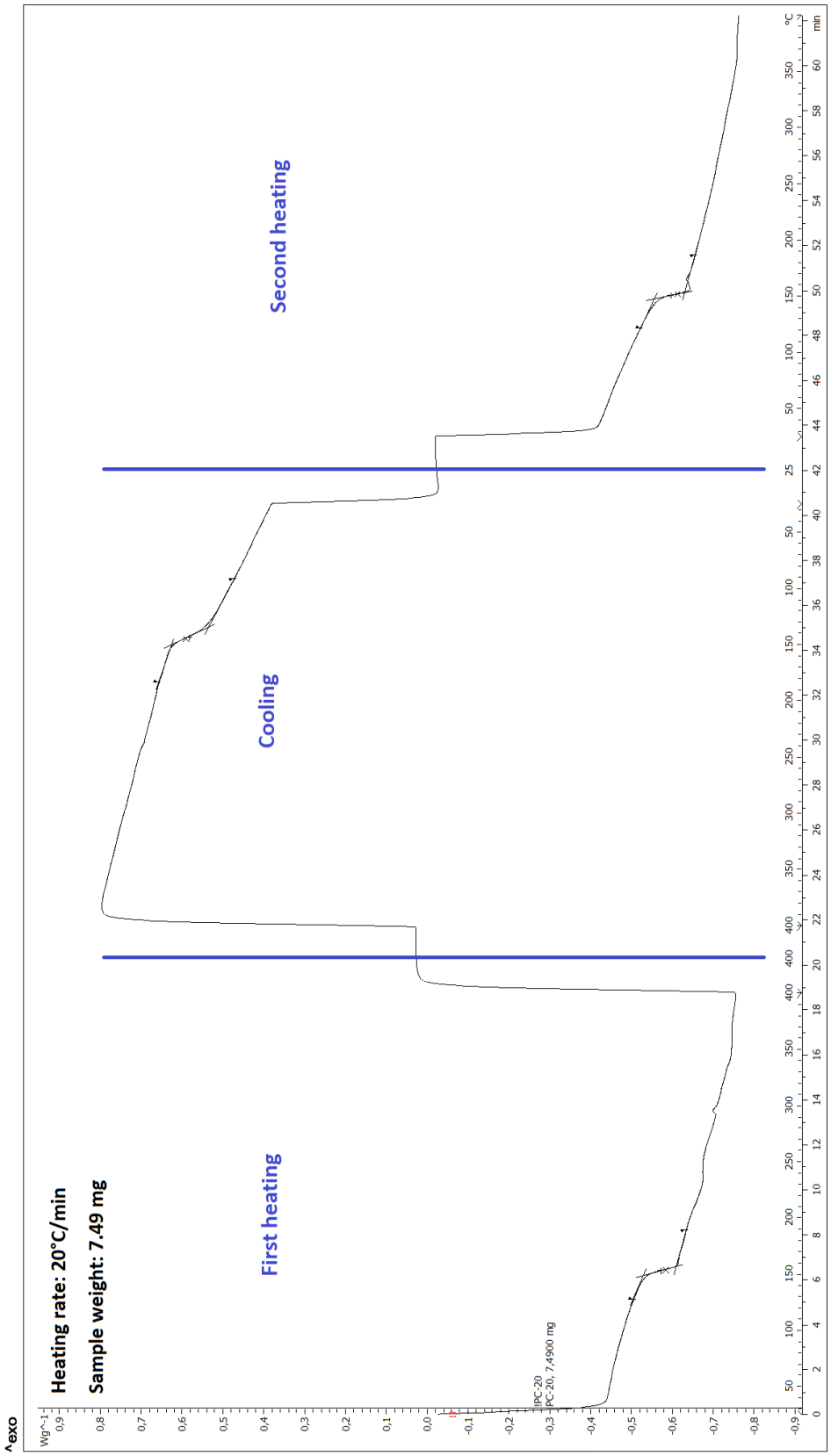

Figure A9. DSC results for a PC sample with a heating/cooling rate of 20°C/min. First heating up to 400°C. Cooling down to 25°C. Second heating up to 400°C.